Microchimica Acta (2021) 188:168
https://doi.org/10.1007/s00604-021-04827-9

REVIEW ARTICLE

State-of-the-art progress of switch fluorescence biosensors based on metal-organic frameworks and nucleic acids

Ya-peng Huo[1,2] · Sha Liu[1] · Zhi-xian Gao[1] · Bao-an Ning[1] · Yu Wang[2]

Received: 19 November 2020 / Accepted: 6 April 2021

Abstract

Metal-organic frameworks (MOFs) have captured substantial attention of an increasing number of scientists working in sensing analysis fields, due to their large surface area, high porosity, and tunable structure. Recently, MOFs as attractive fluorescence quenchers have been extensively investigated. Given their high quenching efficiency toward the fluorescence intensity of dyes-labeled specific biological recognition molecules, such as nucleic acids, MOFs have been widely developed to switch fluorescence biosensors with low background fluorescence signal. These strategies not only lead to specificity, simplicity, and low cost of biosensors, but also possess advantages such as ultrasensitive, rapid, and multiple detection of switch fluorescence methods. At present, researches of the analysis of switch fluorescence biosensors based on MOFs and nucleic acids mainly focus on sensing of different types of in vitro and intracellular analytes, indicating their increasing potential. In this review, we briefly introduce the principle of switch fluorescence biosensor and the mechanism of fluorescence quenching of MOFs, and mainly discuss and summarize the state-of-the-art advances of MOFs and nucleic acids-based switch fluorescence biosensors over the years 2013 to 2020. Most of them have been proposed to the in vitro detection of different types of analytes, showing their wide scope and applicability, such as deoxyribonucleic acid (DNAs), ribonucleic acid (RNAs), proteins, enzymes, antibiotics, and heavy metal ions. Besides, some of them have also been applied to the bioimaging of intracellular analytes, emerging their potential for biomedical applications, for example, cellular adenosine triphosphate (ATP) and subcellular glutathione (GSH). Finally, the remaining challenges in this sensing field and prospects for future research trends are addressed.

Keywords Metal-organic frameworks · Fluorescence quencher · Nucleic acids · Switch fluorescence biosensors · Fluorescence detection · Bioimaging

Introduction

Metal-organic frameworks (MOFs) are a new type of crystalline porous materials formed via the self-assembly of metal nodes and organic ligands by coordination interactions. [1] According to the configuration source, there are many kinds of classification methods of MOFs, such as isoreticular metal-organic frameworks (IRMOFs), zeolitic imidazolate framework materials (ZIFs), and porous coordination networks (PCNs). According to the research team or university name, MOFs include the materials of Institute Lavoisier (MILs) and University of Oslo (UiOs), etc. IRMOFs are self-assembled materials by the $[Zn_4O]^{6+}$ group possessing a series of aromatic carboxylic acid ligands in the octahedral structure (Fig. 1a). [2] ZIFs are zeolite-like structural materials synthesized via the reaction of Zn^{2+} or Co^{2+} and imidazole ligands (Fig. 1b). [3] MILs materials are formed using transition metal elements and dibasic carboxylic acid ligands (Fig. 1c). [4] PCNs possess multiple cubic octahedral nano-cages, which can form pore-channel topology space structure (Fig. 1d). [5] UiOs are generated through the reaction of Zr-containing regular octahedron $[Zr_6O_4(OH)_4]$ and phthalic acid ligand (Fig. 1e). [6] Compared with conventional inorganic porous materials, MOFs exhibit super high specific surface area, ultrahigh

Ya-peng Huo and Sha Liu contributed equally to this work.

✉ Bao-an Ning
ningba@163.com

✉ Yu Wang
wangyu@lzu.edu.cn

[1] Tianjin Key Laboratory of Risk Assessment and Control Technology for Environment and Food Safety, Tianjin Institute of Environmental and Operational Medicine, Tianjin 300050, China

[2] School of Public Health, Lanzhou University, Lanzhou 730000, China

Published online: 21 April 2021

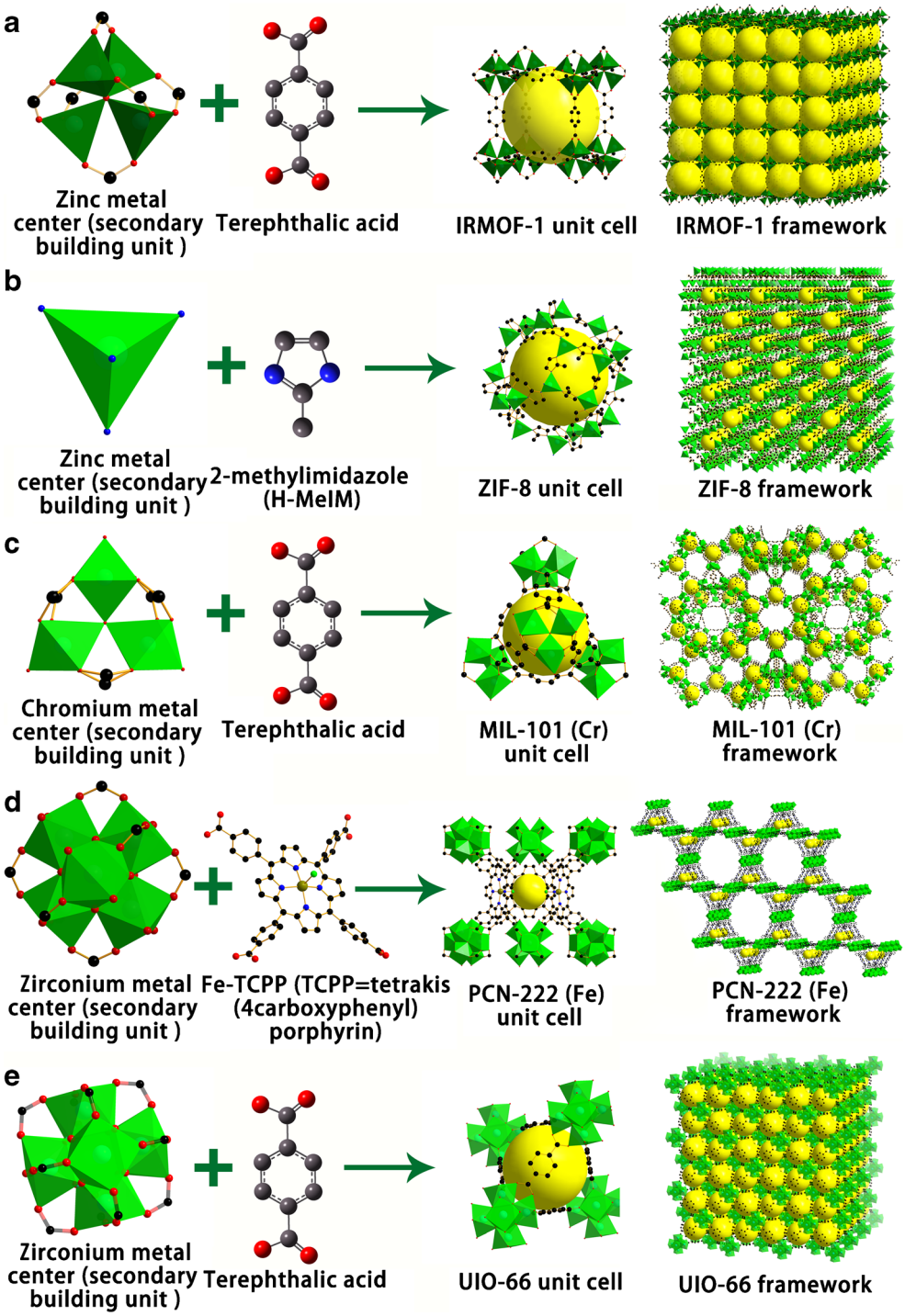

Fig. 1 Representative MOF types. Schematic illustrations of metal centers (secondary building units), organic linkers, unit cells, and frameworks of IRMOF-1 (**a**), ZIF-8 (**b**), MIL-101(Cr) (**c**), PCN-222(Fe) (**d**), and UiO-66 (**e**)

porosity, tunable structures, modified and tailored flexibility, and unique physical and chemical properties. [7] They have promising applications in gas storage [8], separation [9], catalysis [10], imaging [11], drug delivery [12], and enzyme encapsulation [13]. Based on the above superior properties, MOFs also provide an ideal platform for the analysis and research of biosensors that display excellent performances. [14] Over the last decade, MOFs-related researches have grown exponentially (Fig. 2) in the field of biosensors.

Additionally, MOFs as potential fluorescence quencher have been of interest, as well as specific biological recognition molecules through the combination of biomolecules modified by fluorescent dyes. Based on observable changes in fluorescence intensity of dyes before and after adding quenchers,

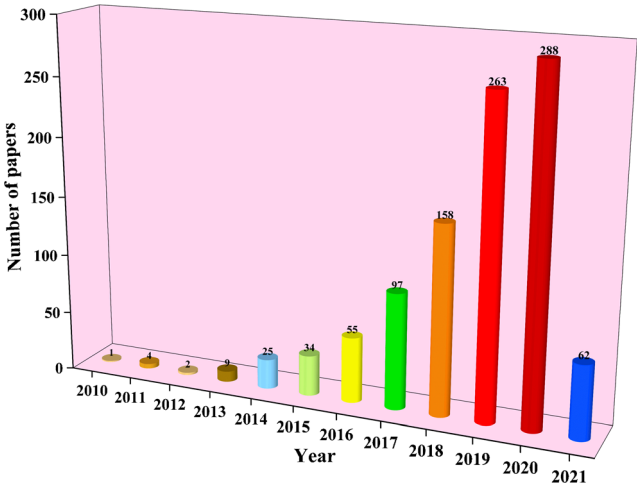

Fig. 2 The number of MOFs-related biosensing research papers published each year from 2010 to 2021. Web of Science of knowledge data by searching topic words of "metal-organic framework" and "biosensing or biosensor" on March 20, 2021

switch fluorescence biosensors have been designed to realize fast, sensitive, and reliable quantitative analysis of a variety of samples. Typical fluorescence quenchers include carbon nanotubes (CNTs) [15], graphene oxide (GO) [16], gold nanoparticles [17], quantum dots [18], and composite materials [19]. Compared with carbon materials, MOFs have characteristically high fluorescence quenching efficiency, short quenching time and good stability, as well as easy synthesis, environmentally friendly and high cost-effectiveness. [20] Given that aforementioned characteristics, MOFs have evolved into ideal materials for analysis sensing, which can obtain high sensitivity and short analysis time when applied in sensing systems. Therefore, the study of application and research of MOFs as fluorescence quenchers in switch fluorescence biosensors is desirable. [21] Among them, fluorescence biosensors that utilize biomolecules as specific biological recognition molecules (for example, nucleic acids, peptides, and enzymes) involve specific binding with target analyte and can realize the specific biological recognition sensing of targets through related biochemical reactions to produce a fluorescence signal response. [22] Furthermore, fluorescence biosensors would be easy to popularize because of their simple design, easy operation, high specificity, and low cost. [23] The progression and development of materials and synthetic technology allowed fluorescence biosensors to become multifunctional, multidiscipline, and generalized when combined with novel materials. In the recent 8 years, the analysis researches of switch fluorescence biosensors based on MOFs and nucleic acids mainly focused on sensing of different types of in vitro and intracellular analytes, indicating their increasing potential applications.

In this review, we briefly introduce the principle of switch fluorescence biosensor and the mechanism of fluorescence quenching of MOFs. The state-of-the-art progresses of MOFs and nucleic acids-based switch fluorescence biosensors are mainly discussed and summarized covering the 2013~2020 time period. They have mostly been proposed to the in vitro detection of different types of analytes, including deoxyribonucleic acid (DNAs), ribonucleic acid (RNAs), proteins, enzymes, antibiotics, and heavy metal ions, showing their wide scope and applicability. Besides, they have also been applied to the bioimaging of intracellular analytes, containing cellular adenosine triphosphate (ATP) and subcellular glutathione (GSH), emerging their potential for biomedical applications. Furthermore, some unresolved challenges, as well as future perspectives in this field, are confronted and proposed. We anticipate that this review will inspire broader interests and more exciting explorations of MOFs and nucleic acids-based switch fluorescence biosensors for advanced applications in materials science, chemistry, medicine, food, and environmental science.

Principle of switch fluorescence biosensors

Switch fluorescence biosensors with high specificity and sensitivity have received extensive interest over the years. Currently, the design of common switch fluorescence biosensor mainly involves three processes: fluorescence dyes-labeled specific biological recognition molecules, fluorescence quencher, and detecting targets. The most commonly used specific biological recognition molecules are aptamers with high affinity and high specificity, which are artificial single-stranded DNAs or RNAs. [24] In addition, with features of easy production, cost-efficient, and satisfactory chemical stability, application of aptamers as specific biological recognition molecules in biosensors is a good alternative of natural receptors such as antibodies and enzymes. Studies have shown the π-π stacking effect between the ring structure of the basic group and material's aromatic rings, [25] as well as the static and coordinative interactions between the phosphate group and metal ions, [26] allowing the aptamer to be absorbed on the material surface. These interactions are highly effective for biosensor analysis.

The basic principle of the design of "on-off" fluorescent biosensors is as follows (Fig. 3b). [27] Firstly, a quencher is used to adsorb the specific biological recognition molecules modified by fluorescent dyes through electrostatic, stacking, coordination, hydrogen bonding, and other interactions. The close proximity between quenchers and specific biological recognition molecules initiates the quenching process of quenchers to fluorescence dyes, leading to the fluorescence quenching and remaining in the "turn off" status (Fig. 3c). Subsequently, specific binding effects occur between the targets and specific biological recognition molecules, forming rigid complexes, which decrease the binding effect between quenchers and fluorescence dye-labeled specific biological

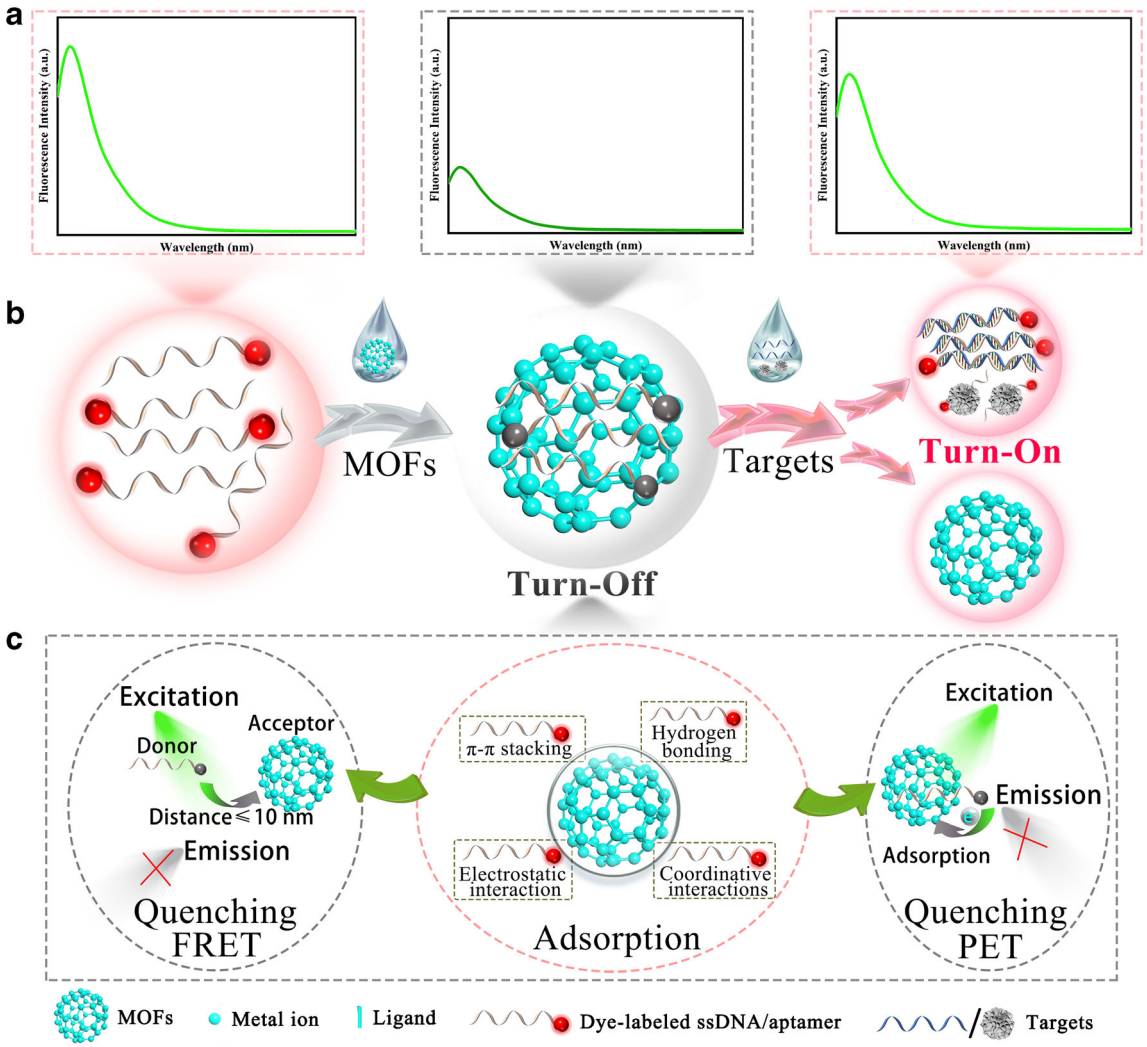

Fig. 3 Principle of switch fluorescence biosensors. Schematic illustrations of fluorescence spectra of switch fluorescence biosensors (**a**), switch fluorescence biosensors with MOFs quenchers and fluorescence dye-labeled specific biological recognition molecules as sensing platforms (**b**), and fluorescence quenching mechanisms of MOFs (**c**)

recognition molecules. This allows for later release from the surface of quenchers, promoting fluorescence recovery while maintaining the "turn on" status. Then the quantitative determination of targets can be realized according to the fluorescence signal change from "off" to "on" before and after combining targets (Fig. 3a). The detection process of the "off-on" type is simple, but compared with "on-off" type fluorescence signal change, such a fluorescence sensor has lower fluorescence background signal and higher signal-to-noise ratio (S/N), which can remarkably improve the detection sensitivity. [28] This method also has good specificity and generality, which enables determination of various targets by changing different specific biological recognition molecules. In addition, the combination of the characteristic properties of the MOFs materials, highly effective and rapid quenching results can be obtained through synergistic effects of various quenching mechanisms, which ultimately improve detection performance.

Fluorescence quenching mechanism of MOFs

Fluorescence quenching or fluorescence intensity decreasing occurs when fluorescence dyes or fluorophores have interaction with quenchers. At present, studied fluorescence quenching mechanisms mainly include six quenching processes. (1) Dynamic and static quenching [29]: the former refers to fluorescence quenching caused by energy transfer or electron transfer of the excited fluorophores and quenchers, in which the excited fluorophores cannot return to the ground state through collision with quenchers. The later refers to the fluorescence quenching caused by the non-fluorescence ground state ligands formed from the fluorophores and quenchers. (2) Förster (or fluorescence) resonance energy transfer (FRET): it is a distance-sensitive energy-transfer process, involving the radiation-less transfer of energy from a "donor" (fluorophore) to an "acceptor" (quencher). The efficiency of energy transfer is inversely proportional to the sixth

power of the distance between donors and acceptors, whereby FRET is extremely sensitive to small distances. Governed by the physics of molecular proximity, FRET can occur when the distance between donors and acceptors are within 1 ~ 10 nm. [30] The efficiency is also dependent on the overlap between the fluorescence spectra of donors and the absorbance spectra of acceptors. Moreover, the fluorescence lifetime of donors can decrease. (3) Photo-induced electron transfer (PET): it is the fluorescence quenching process caused by the electron transfer between the electron donor and electron receptor at an excited state after the electron donor or receptor upon light excited. [31] (4) Ligand-to-metal charge transfer (LMCT): it is the electron of ligand excited by light can transfer to metal center, and then the metal excited state is back to the ground state via nonradiative relaxation. [32] (5) Intramolecular charge transfer (ICT): it is the fluorescence quenching process caused by the electron transfer between the electron-donating group and electron withdrawing group existed within the molecules when both ends of the fluorescence molecule skeleton is connected to the coupling electron-donating group and electron withdrawing group, respectively. [33] (6) Inner filter effect (IFE): it results from the absorption of the excitation or emission radiation by the quencher when the absorption spectra of the quencher overlap with the fluorescence excitation or emission spectra of fluorophores. [34] The process of IFE can result in a reduction of the fluorescence intensity, but the fluorescence lifetime of fluorophores will not be changed.

The presented studies show that the fluorescence quenching mechanisms of MOFs are mainly based on FRET and PET processes (Tables 1 and 2), benefitting from the unique physical and chemical properties of tunable MOF structures. In the case of the FRET mechanism, the organic ligands of the aromatic ring structure contained in MOFs can act as the fluorescence acceptor, in which the absorption spectra of MOFs show a good overlap with the fluorescence emission spectra of fluorophores as well as reducing the fluorescence lifetime. Moreover, as a result of static, π-π stacking, coordination, and hydrogen bonding interactions, the distance between MOFs and fluorophores is shortened. Therefore, fluorescence energy transfer effect can occur from fluorophores to organic ligands. In addition, since most of the MOF structures show semiconductor-like behavior [58, 59], the fluorescence quenching PET mechanism can be explained by the frontier orbital theory, in which highest occupied molecular orbital-lowest unoccupied molecular orbital (HOMO-LUMO) can be called frontier orbital. After the MOFs and fluorophores are excited, the orbital energy levels change in two ways. The electrons of MOFs on HOMO orbitals can transfer to the HOMO orbitals of fluorophores at the excited state, which is the reduced type FET. Or MOF structures containing vacant orbitals can accept electrons, allowing the electrons excited to LUMO orbitals of fluorophores to be transferred to vacant orbitals of MOFs, which is the oxidized type PET. Both types of PET process can impede the excited electrons of fluorophores from returning to the ground state and cause the fluorescence quenching. MOFs have received extensive attention in the presented literatures due to their unique fluorescence quenching properties, which are widely applied in the development of nucleic acids-based switch fluorescence biosensors and possess potential application prospective in the detection field.

In vitro detection of analytes

MOFs have been successfully applied in the construction of nucleic acids-based switch fluorescence biosensors for the in vitro detection of different types of analytes, including DNAs, RNAs, enzymes, proteins, antibiotics, heavy metal ions, and other analytes. To indicate the analytical characteristics of the described biosensors for the in vitro detection of different types of analytes, a brief summary is presented in Table 3.

DNAs

The rapid and sensitive quantitative determination of nucleic acids is significantly important for the diagnosis and treatment of diseases. Traditional detection of nucleic acids mainly relies on amplification-related strategies [73] with sensitivity and specificity, such as polymerase chain reaction (PCR). However, the majority of these techniques requires expensive biochemical reagents and involves time-consuming procedures. Exploration and development of MOFs and nucleic acids-based switch fluorescence biosensors for sensing analysis of DNA molecules has risen exponentially in recent years due to low-cost, simplicity, and sensitivity.

Zeolitic imidazolate frameworks (ZIFs) are effectively used as sensing platforms because of excellent chemical stability and biocompatibility. Especially, ZIF-8 is one of the most promising ZIFs, consisting of zinc ion (Zn^{2+}) and 2-methyl imidazole. Pan et al. utilized ZIF-8 as a sensing platform for the detection of human immunodeficiency virus (HIV)-1 DNA. [40] ZIF-8 possesses exceptional water stability and contains stacking π-electron systems of the bridging five-membered imidazolate ring. Hence, the fluorescence of fluorophore carboxyfluorescein (FAM)-labeled single-stranded DNA (ssDNA) was strongly adsorbed by π-π stacking and electrostatic interaction, and then quenched due to the PET process. Its linear range was from 10 to 100 nmol/L. The limit of detection (LOD) was as low as 1.2 nmol/L calculated by 3σ/slope, where σ was the standard deviation (SD) of 15 blank measurements and slope represented the slope of the calibration plot. Moreover, the HIV-1 DNA indicated much higher target-dependent recovery fluorescence intensity than one, two, and three-base-mismatched ssDNA. These results

Table 1 A summary of the characteristics of various MOFs

MOFs	Metal compounds	Organic compounds	Structure	QEs (%)	Quenching time (min)	Quenching mechanisms	Ref.
UiO-66	Zirconium(IV) chloride ($ZrCl_4$)	1,4-Benzenedicarboxylic acid (H_2BDC)	3D	82	–	PET	[35]
UiO-66-NH_2	$ZrCl_4$	2-Amino-1,4-benzenedicarboxylic acid (NH_2-H_2BDC)	3D	56	20	PET	[36]
PCN-222	$ZrCl_4$	Tetrakis(4-carboxyphenyl)porphyrin (H_2TCPP)	3D	>95	1	PET+FRET	[20]
PDA/UiO-66	$ZrCl_4$	H_2BDC	3D	99	–	PET+FRET	[37]
Fe_3O_4/MIL-88A	Iron(III) nitrate nonahydrate ($Fe(NO_3)_3{\cdot}9H_2O$)	Fumaric acid	3D	>90	5	PET+FRET	[38]
MIL-88B	$Fe(NO_3)_3{\cdot}9H_2O$	H_2BDC	3D	nearly 100	1	PET	[27]
MIL-101(Cr)	Chromium(III) nitrate nonahydrate ($Cr(NO_3)_3{\cdot}9H_2O$)	H_2BDC	3D	nearly 100	100	PET+FRET	[39]
ZIF-8	Zinc(II) nitrate hexahydrate ($Zn(NO_3)_2{\cdot}6H_2O$)	2-Methyl imidazole	3D	66	60	PET	[40]
Zr-MOF	$ZrCl_4$	H_2TCPP	3D	81	5	PET	[41]
$[Cu(Dcbcp)(bpe)]_n$	Copper(II) sulfate pentahydrate ($CuSO_4{\cdot}5H_2O$)	*N*-(3,5-dicarboxylbenzyl)-(3-carboxyl) pyridinium (H_3DcbcpBr), 1,2-bis(4-pyridyl)ethylene (bpe)	3D	92	–	Contact quenching	[42]
Cu(H_2dtoa)	$CuSO_4{\cdot}5H_2O$	*N*,*N*′-bis(2-hydroxyethyl)dithiooxamide (H_2dtoa)	2D	74.5	20	FRET	[43]
Cu-TCPP	Copper(II) nitrate trihydrate ($Cu(NO_3)_2{\cdot}3H_2O$)	H_2TCPP	2D	85	–	FRET	[44]
Fe_3O_4/g-C_3N_4/HKUST-1	$Cu(NO_3)_2{\cdot}3H_2O$	1,3,5-Benzenetricarboxylic acid (H_3BTC)	3D	87	30	PET	[45]
$[Ba_2(L)(H_2O)]{\cdot}(DMF)_{0.5}(H_2O)_3$	Barium nitrate ($Ba(NO_3)_2$)	Bis-(3,5-dicarboxy-phenyl)terephthalamide (H_4L)	3D	94	10	Contact quenching	[46]
$\{[La_2(Cbdcp)_3(H_2O)_{10}]\}_n$	Lanthanum(III) nitrate hexahydrate ($La(NO_3)_3{\cdot}6H_2O$)	*N*-(4-carboxybenzyl)-3,5-dicarboxylpyridinium bromide (H_3CbdcpBr)	2D	57	–	PET	[47]
$Cd(L){\cdot}(HDMA)_2(DMF)(H_2O)_3$	Cadmium(II) chloride monohydrate ($CdCl_2{\cdot}H_2O$)	H_4L	3D	92	30	PET	[48]
$Zn(L){\cdot}(HDMA)_2(DMF)(H_2O)_6$	$Zn(NO_3)_2{\cdot}6H_2O$		3D	97	30		
$[Fe(4\text{-}PyP)(H_2O)][Pt(CN)_4]{\cdot}H_2O{\cdot}CH_3OH$	Iron(II) Perchlorate Hexahydrate ($Fe(ClO_4)_2{\cdot}6H_2O$) and Potassium tetracyanoplatinate(II) hydrate ($K_2Pt(CN)_4{\cdot}3H_2O$)	Diethyl 4-pyridylphosphonate (4-PyP)	2D	91	10	LMCT	[49]

En dash denotes “not reported”

Table 2 Application of 2D MOFs and nucleic acids-based switch fluorescence biosensors in DNAs detection

MOFs	Quenching mechanisms	QEs (%)	Specific biological recognition molecules	DNAs	Limit of detection[a] (nmol/L)	Linear range (nmol/L)	Ref.
$\{[Zn(HCbdcp)_2]\cdot H_2O\}_n$	PET	73	FAM-ssDNA	HIV DNA	1×10^{-2}	1~80	[50]
$Mn(C_6H_8O_4)(H_2O)$	–	–	TAMRA-ssDNA	*Homo sapiens* tumor suppressor gene	2×10^{-4}	1×10^{-3}~0.2	[51]
$[Cu(Dcbb)_2]_n$	PET	61.8	FAM-ssDNA	HIV DNA	1×10^{-3}	$1\sim1.2\times10^{2}$	[52]
$Cu(H_2dtoa)$	PET	84.5	FAM-ssDNA	HIV DNA	3	$10\sim1\times10^{2}$	[53]
$Cu(H_2dtoa)$	–	85.0 91.1	FAM-ssDNA ROX-ssDNA	HBV DNA HIV DNA	0.87 0.22	1~10	[54]
$Cu(H_2dtoa)$	PET	80.7	FAM-probe triplex-forming oligonucleotide	DNA (polypurine tract sequence of HIV-1 RNA)	1.3	$4\sim2\times10^{2}$	[55]
Cu-TCPP	FRET	89	Texas Red-ssDNA	Influenza A virus subtype H_5N_1 gene	2×10^{-2}	2×10^{-2}~5	[56]
Cu-TCPP	FRET	97	Texas Red-ssDNA Cy3-ssDNA FAM-ssDNA	*Salmonella enterica* DNA *Listeria monocytogenes* DNA *Vibrio parahemolyticus* DNA	2.8×10^{-2} 3.5×10^{-2} 1.5×10^{-2}	0.5~15 0.1~12 0.1~9	[57]

En dash denotes "not reported"

[a] The limit of detection is defined as S/N = 3

showed that this sensing platform could be applied for highly selective determination of DNA sequences in vitro. However, in this case, ZIF-8 showed poor fluorescence quenching property, with only 66% quenching efficiency (QE) in 60 min. Therefore, in order to obtain excellent fluorescence quenching behavior of nano-quenchers, lanthanide ions (Lns) were doped into a nanoscale ZIF-8 structure [60] (Fig. 4a). Lns were lanthanum ion (La^{3+}), cerium ion (Ce^{3+}), neodymium ion (Nd^{3+}), and terbium ion (Tb^{3+}), respectively. Nanoscale ZIF-8 (about 300 nm) was selected as a fluorescent sensing platform because its particle size can be easily regulated by changing the reaction solvent at room temperature. This study showed that the fluorescence quenching ability of La^{3+} doped ZIF-8 (ZIF-8-La) was around threefold higher than that of ZIF-8 (Fig. 4b). Furthermore, core-shell La^{3+} doped ZIF-8 (CS-ZIF-8-La) was synthesized to decorate more La^{3+} on the surface of ZIF-8, the thickness of whose shell was around 20 nm. As shown in Fig. 4c, the fluorescence of dyes displayed enhanced quenching by CS-ZIF-8-La. These fluorescence behaviors were related to the charge property of fluorophores labeled on ssDNA. The fluorescence intensity of the fluorophores was quenched by three types of MOFs. After interactions with target DNA, the fluorescence of positive-dye labeled ssDNA was recovered, such as tetramethylrhodamine (TAMRA) and Texas red. In contrast, CS-ZIF-8-La further quenched the fluorescence of negative-dye labeled ssDNA, such as FAM and Cy5, which was consistent with their previous work [74]. This was due to the formed negative-dye labeled double-stranded DNA (dsDNA) could not leave away from the CS-ZIF-8-La surface, but recombined with the substantial La^{3+} because of electrostatic interaction, resulting in lower fluorescence signals. Based on CS-ZIF-8-La as a fluorescence quenching platform, the ratiometric sensors were designed for the determination of DNA with the linear range of 1 ~ 30 nmol/L (Fig. 4d). The CS-ZIF-8-La ratiometric aptameric platform was also used for detecting microRNA-21 (miR-21). Interestingly, the ratios induced by miR-21 were much higher than that caused by other microRNAs (miR-141, miR-21-5p, and let-7a) or biomolecules (adenosine, uridine, and cytosine triphosphate), suggesting the high specificity of sequence probe and application prospect in complex biosystems. The ratiometric sensors could open up an exciting new avenue for the construction of fluorescence biosensors.

Iron- and zirconium-containing MOFs (Fe-MOFs and Zr-MOFs, respectively) have been extensively employed owing to their many advantageous attributes, such as fascinating properties and chemical versatility. One typical feature of such MOFs is Fe and Zr unsaturated metal centers, which exhibit strong Fe-O and Zr-O coordination bonds between unsaturated metal centers and O atoms in the organic ligands. These endow Fe-MOFs and Zr-MOFs with preferable stability for sensing systems. [58, 75] More importantly, the Fe^{3+} or Zr^{4+} metal centers possess high electron-accepting ability serving as electron-consuming pools to boost the electronic transfer, which could improve the quenching efficiency. By integrating these metal centers and benzene-containing organic ligands with conjugated π-electron structures, MOFs can achieve greatly enhanced fluorescence quenching action through the utilization of the synergistic effect between metal centers and organic ligands. MIL-88B nanorods, synthesized using Fe^{3+} and 1,4-benzenedicarboxylic acid (H_2BDC), were developed

Table 3 Application of MOFs and nucleic acids-based switch fluorescence biosensors for the in vitro detection of different types of analytes

Types of analytes	Analytes	MOFs	Limit of detection	Linear range	Real sample	Spiked recovery (%)	Ref.
DNAs	HIV DNA	ZIF-8	1.2 nmol/L	10~100 nmol/L	–	–	[40]
	ssDNA (a model chain of tumor suppressor genes)	CS-ZIF-8-La	0.37 nmol/L	1~30 nmol/L	–	–	[60]
	HIV DNA	MIL-88B	10 pmol/L	$10\sim5\times10^3$ pmol/L	–	–	[27]
	HIV DNA	MIL-88A	1 nmol/L	3~150 nmol/L	Fetal bovine serum	98.20~106.79	[38]
	HIV DNA	MIL-101(Cr)	73 pmol/L	0.1~14 nmol/L	–	–	[61]
RNAs	Ebolavirus conserved RNA sequences	$\{[Cu(Cmdcp)(phen)(H_2O)]_2{\cdot}9H_2O\}_n$	163 pmol/L	$163\sim6\times10^4$ pmol/L	–	–	[62]
	Ebolavirus-encoded miRNA-like fragment		111 pmol/L	$111\sim6\times10^4$ pmol/L			
	DENV RNA sequences	$[Cu(Dcbcp)(bpe)]_n$	332 pmol/L	$1\times10^3\sim6\times10^4$ pmol/L	–	–	[42]
	ZIKV RNA sequences		192 pmol/L	$5\times10^2\sim7\times10^4$ pmol/L			
	miR-185, miR-20a, miR-92b, miR-25, miR-210	$\{[Cu(dcbb)_2(H_2O)_2]{\cdot}10H_2O\}_n$	172, 321, 91, 559, 132 pmol/L	$172\sim8\times10^4$, $321\sim1\times10^5$, $91\sim1\times10^5$, $559\sim7\times10^4$, $132\sim8\times10^4$ pmol/L	–	–	[63]
	miR-21, miR-96, miR-125b	UiO-66	10 pmol/L	10~1000 pmol/L	–	–	[35]
Proteins	H_5N_1 antibody	$Cu(H_2dtoa)$	1.6×10^{-9} mol/L	$1\times10^{-9}\sim1\times10^{-6}$ mol/L	Human serum	94~102	[64]
	PSA	Zr-MOF@AuNP@GO	0.01 ng/mL	0.05~10 ng/mL	Human serum	–	[41]
Enzymes	ALP	Ce^{3+}/Ce^{4+}-based MOF (MVCM)	0.18 mU/mL	2~100 mU/mL	Human serum	95.65~100.60	[65]
	DNase I	$[Ba_2(L)(H_2O)]{\cdot}(DMF)_{0.5}(H_2O)_3$	0.04 U/mL	0.1~10 U/mL	Cell lysate	98.0~102.7	[46]
Antibiotics	CAP	PCN-222	0.08 pg/mL	$0.1\sim1\times10^4$ pg/mL	Milk and shrimp	89.91~106.15	[20]
	KANA	PDA-based MOF (ZIF-67)	0.304 nmol/L	0.304~50 nmol/L	Milk	96~101	[66]
	OTC		0.481 nmol/L	0.481~50 nmol/L		95~100	
	CAP	Cu-TCPP	1.5 pmol/L	$5\sim1\times10^4$ pmol/L	Milk	91~101	[67]
	OTC		2.4 pmol/L	$8\sim5\times10^4$ pmol/L			
	KANA		1 pmol/L	$3\sim3\times10^4$ pmol/L			
	CAP	Cu-TCPP	0.3 pg/mL	$1\sim1\times10^4$ pg/mL	Milk and fish	93.67~106.08	[44]
	OTC	MIL-101(Cr)	4.2 nmol/L	$10\sim2\times10^3$ nmol/L	Duck	77.2~87.9	[39]
Heavy metal ions	Hg^{2+}	PDA coated ZIF-67 (MPDA)	1.3×10^{-3} nmol/L	$1.3\times10^{-3}\sim2$ nmol/L	Tap and river water	96.3~100.9	[68]
	Ag^+		3.4×10^{-2} nmol/L	1~3 nmol/L		97.4~101.3	
	Hg^{2+}	NH_2-MIL-101(Fe)@Fe_3O_4	8 nmol/L	2~20 nmol/L	Tap water	around 70	[69]
Others	Gly	$[Cu(mal)(bpy)]{\cdot}2H_2O$	0.81 μg/mL	0.81~100 μg/mL	Newborn bovine serum	95.87~106.60	[70]
	Ser		1.51 μg/mL	5~500 μg/mL			
	BPA	Fe-MIL-88B-NH_2	4.1×10^{-14} mol/L	$5\times10^{-14}\sim2\times10^{-9}$ mol/L	–	–	[71]
	E. coli O157:H7	UiO-66	40 CFU/mL	$1.3\times10^2\sim6.5\times10^4$ CFU/mL	Spring water, skim milk, and orange juice	95.72~105.52	[72]
	ATP	PDA-coated Zr-MOF (PDA/UiO-66)	35 nmol/L	$35\sim1\times10^3$ nmol/L	–	–	[37]
	OTA	Fe_3O_4/g-C_3N_4/HKUST-1	2.57 ng/mL	5~160 ng/mL	Corn	96.5~101.4	[45]

En dash denotes "not reported"

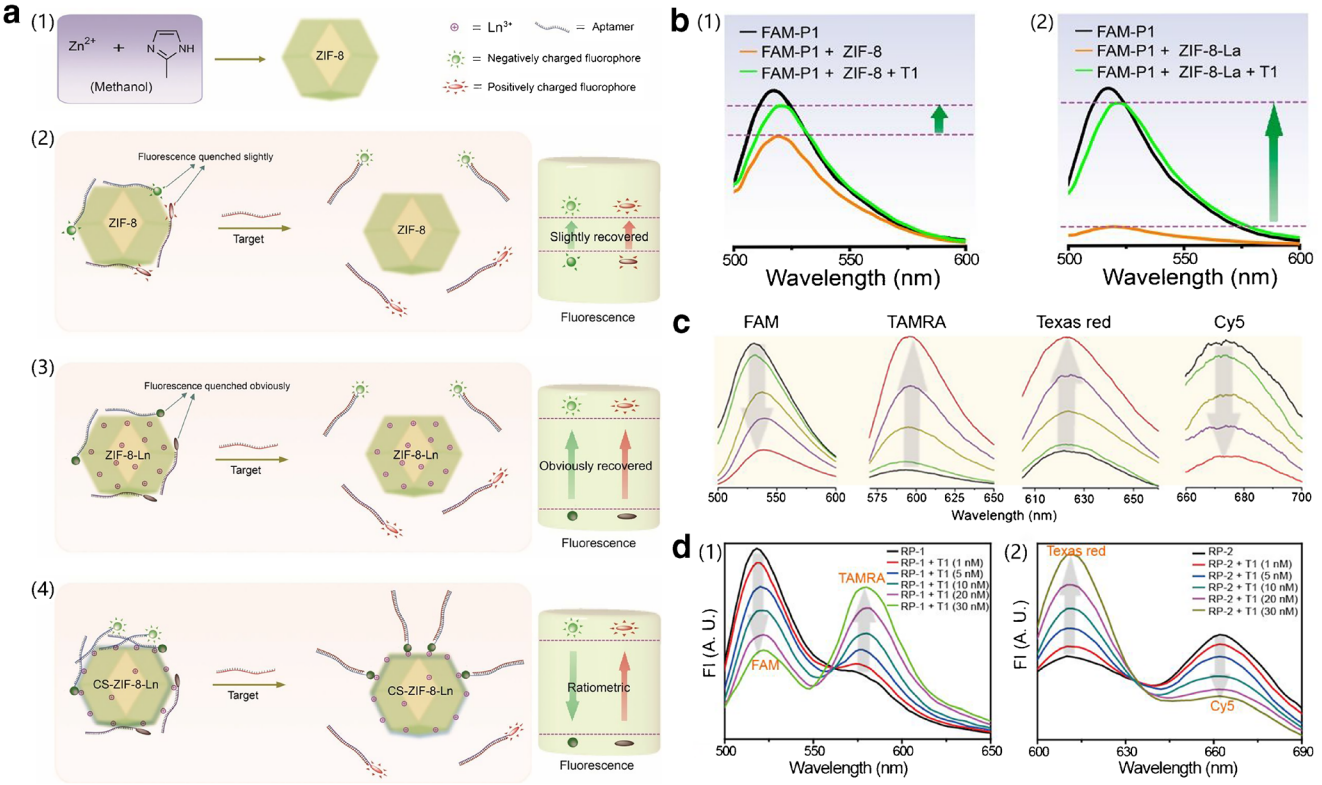

Fig. 4 Lanthanide ions doped ZIF-8 platform for fluorescent biosensing [60]. Copyright 2019, American Chemical Society. **a** Schematic illustration of the fluorescent sensing on ZIF-8 or lanthanide ion (Ln^{3+}) doped ZIF-8. (1): Preparation of ZIF-8. (2-4): Target-induced probe fluorescence change on ZIF-8 (2), ZIF-8-Lns (3), and CS-ZIF-8-Lns (4). **b** Fluorescence spectra of FAM-ssDNA mixed with ZIF-8 (1) or ZIF-8-La (2) by adding DNA. **c** Fluorescence spectra of different dye-labeled ssDNA (FAM, TAMRA, Texas red, and Cy5) mixed with CS-ZIF-8-La containing DNA with different concentrations (the lines of black, green, yellow, purple, and red were 0, 10, 20, 50 nmol/L for target DNA, respectively). **d** Fluorescent spectral changes of FAM/TAMRA-ssDNA (1) and Cy5/Texas red-ssDNA (2) on CS-ZIF-8-La containing DNA with different concentrations

as a high-efficient fluorescence sensing platform for DNA detection. [27] Based on the adsorption of H_2BDC organic linker and PET process of Fe^{3+} centers, FAM-ssDNA fluorescence was quenched by MIL-88B nanorods with nearly QE of 100%. This DNA sensor exhibited a linear range from 0.01 to 5 nmol/L with low detection limit of 10 pmol/L (3 times the SD in the blank solution), and the strong discrimination of single point mutation. The overall determination time was only 4 min covering 1 min for quenching and 3 min for DNA incubation, implying the superior ability of the sensor. The fluorescence intensity changes of this sensor toward single base mutated ssDNA were about 39% of that toward the target HIV ssDNA while non-complementary ssDNA showed only very small change, showing a high discrimination of single base mutation. Similarly, because amino-containing organic linkers usually have conjugated π-electron systems and significantly offer hydrogen bonds interaction between MOFs and ssDNA, highly sensitive and selective detection of HIV DNA was obtained by employing amine-functionalized MOF (UiO-66-NH_2) as an effective fluorescent sensing platform. [36] UiO-66-NH_2 synthesized by Zr^{4+} and 2-amino-1,4-benzenedicarboxylic acid (NH_2-H_2BDC) exhibits great chemical and thermal stability. Their sizes were in the range of 50 ~ 100 nm, suitable for dispersion in the aqueous solution. The recovered fluorescence intensity of the UiO-66-NH_2 sensor with the complementary target T_1 and single-base mismatched sequence T_2 were 67 and 26%, respectively, compared to 58 and 56% for UiO-66 system. These observations demonstrated that the UiO-66-NH_2 sensing platform was able to distinguish the complementary and single-base mismatching targets, whereas the same structure UiO-66 without an amino group cannot realize such a function. The high selectivity and good reproducibility were attributed to hydrogen bonds interaction between the amino group in UiO-66-NH_2 and ssDNA bases. Besides, our group constructed a UiO-66 based fluorescence sensing assay for the detection of DNA and *Escherichia coli* O157:H7 (*E. coli* O157:H7) through clustered regularly interspaced short palindromic repeats-Cas9 (CRISPR-Cas9) triggered two-step isothermal amplification method. [72] As shown in Fig. 5a, CRISPR-Cas9 system could recognize and cleave target virulence gene sequences, and trigger the strand displacement amplification (SDA) and rolling circle amplification (RCA). After this dual amplification, abundant products could hybridize with FAM-

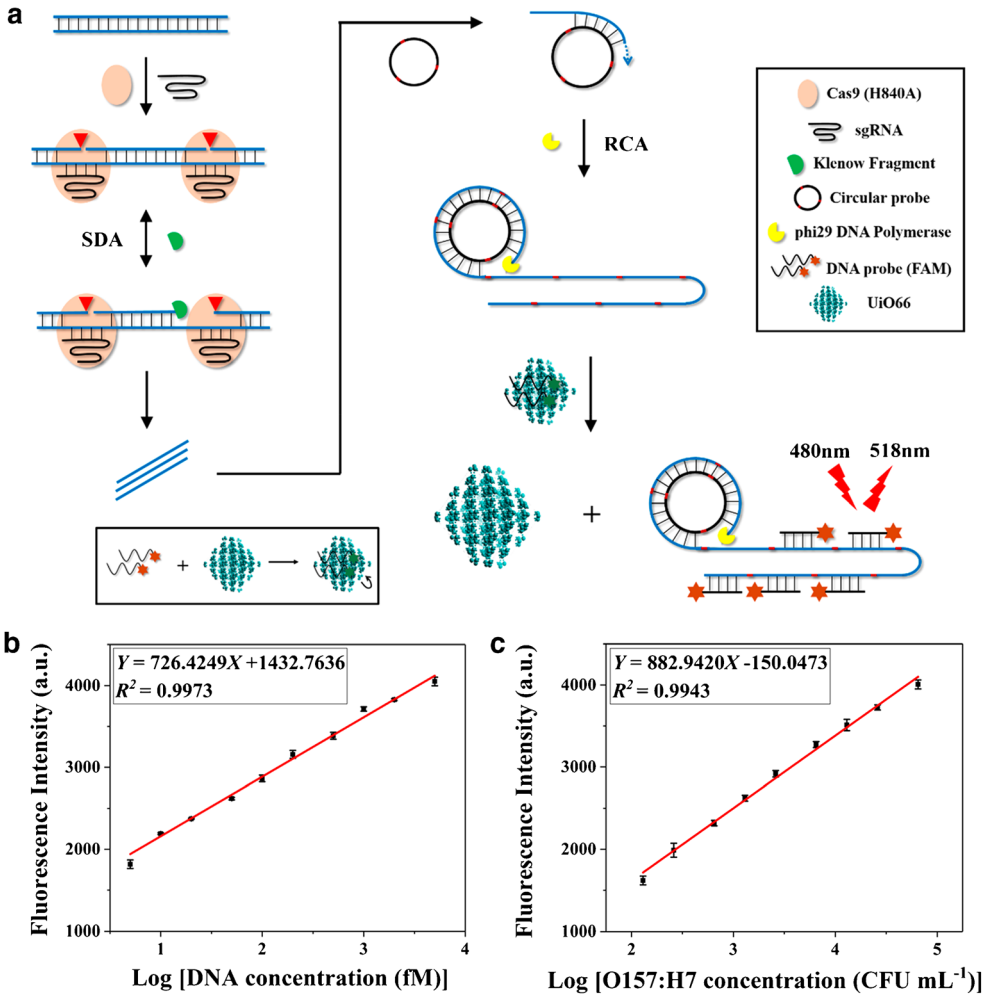

Fig. 5 CRISPR-Cas9 triggered SDA-RCA method for DNA and *E. coli* O157:H7 detection based on the UiO-66 platform [72]. Copyright 2020, American Chemical Society. **a** Schematic illustration of fluorescence sensing determination. **b** Linear relationship between the fluorescence intensity and the logarithm of DNA concentrations ($5 \sim 5 \times 10^3$ fmol/L). **c** Linear relationship between the fluorescence intensity and the logarithm of *E. coli* O157:H7 concentrations ($1.3 \times 10^2 \sim 6.5 \times 10^4$ CFU/mL)

ssDNA probes whose fluorescence was quenched in advance by the UiO-66 platform. Therefore, DNA and *E. coli* O157:H7 was quantitatively determined through the recovery fluorescence intensity. As shown in Fig. 5b, the detection limit of DNA was estimated to be 1.87 fmol/L (the average signal of the blank value plus three times the SD) with a good linear range of $5 \sim 5 \times 10^3$ fmol/L. Compared with previous *E. coli* O157:H7 determination methods, the presented strategy showed a wide range of $1.3 \times 10^2 \sim 6.5 \times 10^4$ CFU/mL (Fig. 5c) and high sensitivity with detection limit of 40 CFU/mL (the average response corresponding to the sample blank value plus three times the SD), which was threefold orders of magnitude lower than real-time PCR Kit (2.6×10^4 CFU/mL). Also, this method exhibited high specificity and accuracy for sensing of practical samples (spring water, skim milk, and orange juice). These distinctive advantages arose due to the following. First, two-step isothermal amplification for dual signal amplification was specifically triggered by CRISPR-Cas9. Second, UiO-66 with significant efficiency reduced the background signal of fluorescence probes. Hence, this method had great potential for further application in food safety and clinical diagnostics. In addition, MOF-derived nanocomposites had highly ordered structures, excellent stability, and repeatability, which can endow the nanocomposites with some enhanced properties. Tan et al. prepared a magnetic porous carbon (MPC) nanocomposite using a precursor of Fe-MOF (MIL-88A). [38] MPC-induced complete quenching of FAM-ssDNA fluorescence within 10 min was attributed to the synergetic effect of magnetic nanoparticles and carbon matrix, resulting in FRET and PET processes. The proposed biosensor exhibited a linear range of $3 \sim 150$ nmol/L and detection limit of 1 nmol/L, which was calculated on the basis of a signal to noise ratio of 3:1 ($S/N = 3$). It also showed high selectivity toward specific target HIV DNA and even distinguished single-base mismatched sequence. Moreover, the concentration levels of target DNA in spiked fetal bovine serum (FBS) samples were measured accurately with the spiked recoveries of $98.20 \sim 106.79\%$. All of relative standard deviations (RSDs, $n = 5$) were less than 1.57%, showing a wider application in real bioanalysis.

Two MOFs were synthesized using cadmium and zinc metal ions (Cd^{2+}, Zn^{2+}) and bis-(3,5-dicarboxy-phenyl) terephthalamide (H_4L) ligand. [48] H_4L with aromatic structure and amide group could enhance the flexibility of

frameworks and form π-π stacking interaction and additional hydrogen bonding with FAM-ssDNA, which facilitated the PET process. Analysis of the reported biosensor showed that 0.05 nmol/L of target DNA could be determined with the range of 0.05 ~ 125 nmol/L. The selectivity of this sensing platform could be down to a single nucleotide mismatch, applicable for the practical detection of DNA sequences. To avoid the expensive and time-consuming functionalization of fluorophores-labeled probes, Fang et al. developed a label-free and sensitive fluorescence biosensor for DNA determination based on DNA-intercalating dye and MIL-101 ($Cr_3F(H_2O)_2O[(O_2C)\text{-}C_6H_4\text{-}(CO_2)]_3\cdot nH_2O$). [61] The well-known MIL-101 possesses good stability in water with neutral conditions, high surface area, and large pore size. This described MIL-101 could greatly decrease the high fluorescence background of SYBR Green I and probe DNA complex (SG/P). QE of MIL-101 was up to 88.81%, and the signal-to-noise (S/N) ratio displayed an eightfold improvement. The detection limit was 73 pmol/L (3σ) with a good linear range of 0.1 ~ 14 nmol/L. In the presence of MIL-101, one-base-mismatched in target DNA sequence can be discriminated more efficiently from the complementary target DNA. Moreover, due to the stable dsDNA structure between target DNA and its complementary DNA, the fluorescence signal of this system was not affected by the coexisting interfering proteins (pancreatin, bovine serum albumin, alkaline phosphatase, pepsin, prion protein, snailase, lysozyme, and cellulase). Since MIL-101 was a three-dimensional (3D) octahedral shape and can distinguish ssDNA and dsDNA more easily, this method demonstrated that its sensitivity and selectivity was much superior than that based on carbon nanotubes and graphene oxide quenching sensors.

In addition to the above 3D MOFs-based fluorescence biosensors, exploration into other two-dimensional (2D) MOFs has been reported. These nanosheets possess many promising features originating from their ultrathin thickness and 2D morphology. Their surface possesses abundant accessible active sites, which are vital for sensing applications. [76, 77] For example, Hofmann-type MOFs (hMOFs) are a versatile class of materials with a $M^1[M^2(CN)_y]$ network, in which, the M^1 and M^2 are both transition metals with octahedral and square planar coordination, respectively. [78] The structure of hMOFs can be regulated by intermolecular interactions to downsize to nanosheets. [79] Notably, the exposed metal ions of nanosheets have exclusive axial coordination sites with fluorophores for signal switching. Consequently, two hMOFs with 2D monolayer nanosheet structure were precisely synthesized through modulation of the position with phosphonate groups on rigid ligands, which included $[Fe(4\text{-}PyP)(H_2O)][Pt(CN)_4]\cdot H_2O\cdot CH_3OH$ (hMOF-1, 4-PyP = diethyl 4-pyridylphosphonate) and $[Fe(3\text{-}PyP)][Pt(CN)_4]$ (hMOF-2, 3-PyP = diethyl 3-pyridylphosphonate), respectively. [49] Axial coordination occurs between open Fe^{2+} sites of hMOF-1 nanosheets and fluorophores. The monolayer nanosheet possessed 91% fluorescence quenching efficiency via the LMCT quenching mechanism. The FAM-ssDNA was developed as a fluorescence probe for DNA detection. Its quantitative determination was achieved with a linear range of 1 ~ 40 nmol/L and LOD of 0.3 nmol/L (3σ). More remarkably, hMOF-1 nanosheets revealed an excellent selectivity toward single-base mismatched DNA, providing a unique strategy for biosensing. To illustrate their recent applications of 2D MOFs in DNAs detection, a brief summary is presented in Table 2.

RNAs

The majority of common fatal human pathogens are single-stranded RNA virus, such as the Ebola virus (EBOV) and Zika virus (ZIKV). These viruses cause human epidemic diseases with high risk of death, which can pose extremely serious risks to human health and life. Consequently, sensitive and timely determination of RNA virus is a crucial key for rapid diagnosis, prevention, and control of diseases. Currently, the reverse transcription PCR (RT-PCR) and fluorescence quantitative real-time PCR (qRT-PCR) are common amplification methods in clinical settings. Although they satisfy requirements of detection capability, they remain costly, easy-polluting, and time-consuming. [80] As a result, Yang et al. proposed a water-stable 3D Cu-MOF from a tritopic quaternized carboxylate and 4,4′-dipyridyl sulfide as the ancillary ligand. The $[Cu_3(Cmdcp)_2(dps)_4(H_2O)_4(SO_4)]_n$ (**1**, H_3CmdcpBr = *N*-carboxymethyl-3,5-dicarboxylpyridinium bromide; dps = 4,4′-dipyridyl sulfide) featured a notable Kagomé cross-section lattice. [81] More bigger pores can be synthesized by flexible zwitterionic carboxylates of low symmetry to detect longer DNA or RNA sequences. The MOF with unique pore shapes could adsorb two different FAM-ssDNA probes via electrostatic, π-π stacking, and hydrogen-bonding interactions, and then quench the fluorescence of FAM through the PET process. This system achieved the selective determination of Sudan virus (SUDV) RNA sequences and HIV-1 dsDNA, respectively, with detection limits of 73 and 196 pmol/L (S/*N* = 3), respectively. The effect of the longer length of target sequences was also investigated. The results indicated SUDV RNA sequences with up to 80 bases were efficiently detected with no interference of a mutated base. This proposed biosensor could have potential application in virus-associated infectious diseases. Moreover, their research team also developed a sensitive and selective fluorescence biosensor for the simultaneous detection of ebolavirus conserved RNA sequences and ebolavirus-encoded miRNA-like fragment, based on a 3D Cu-MOF of $\{[Cu(Cmdcp)(phen)(H_2O)]_2\cdot 9H_2O\}_n$ (**1**, phen = phenanthroline). [62] The detection limits of 63 and 111 pmol/L (S/N = 3) were obtained with the detection time of 11.8 and 3.1 min, respectively. There was no cross-reaction

of sensing systems for target RNA detecting. As such, Qin et al. reported a 3D dysprosium-based MOF ($\{[Dy(Cmdcp)(H_2O)_3](NO_3)\cdot 2H_2O\}_n$) from a zwitterionic carboxylate. [82] Since the 3D MOF possessed chair-type pore shapes with tessellating H_2O and free NO_3^- anions on their surface, it was moisture and water-stable. These unique structural features provided electrostatic, π-π stacking, and hydrogen bonding interactions with FAM-ssDNA, and then quench its fluorescence through PET process. This fluorescence biosensor could determine complementary ebolavirus RNA sequences as low as 160 pmol/L, which was calculated from the 3σ/slope (σ = SD of five blank measurements). The highly selective sensing ability was satisfactorily evaluated under acidic (pH 6.4), neutral (pH 7.4), and basic (pH 8.0) conditions. Because lanthanides own the attractive oxophilicity and high coordination number to make water-stable and intriguing MOF structures, Yang et al. further explored a 3D MOF of $\{[La_4(Cmdcp)_6(H_2O)_9]\}_n$ (**1**) and a 2D MOF of $\{[La_2(Cbdcp)_3(H_2O)_{10}]\}_n$ (**2**, H_3CbdcpBr = *N*-(4-carboxybenzyl)-3,5-dicarboxylpyridinium bromide). [47] These multidentate carboxylate ligands containing an sp^3 methylene group generally can lower the symmetry of ligands, while they were effectively compensated with a high coordination number of lanthanum ions. Therefore, both MOFs **1** and **2** showed larger pore sizes or larger surfaces to absorb FAM-ssDNA, and quench FAM fluorescence by PET process. Furthermore, they allowed for the determination of SUDV conservative sequences with low detection limits of 112 and 67 pmol/L (S/*N* = 3), respectively. These biosensors also suggested their high selectivity and discriminated RNA sequences down to single-base mismatch. Through single and synchronous fluorescence analysis, simultaneous determination of Dengue virus (DENV) and ZIKV RNA sequences was presented based on a new MOF of $[Cu(Dcbcp)(bpe)]_n$ (**1**, H_3DcbcpBr = *N*-(3,5-dicarboxylbenzyl)-(3-carboxyl) pyridinium, bpe = 1,2-bis(4-pyridyl)ethylene). [42] To build the porous 3D MOF structure with water solubility and stability, an ancillary bridging ligand bpe was introduced into the construction of the Cu(II) zwitterionic carboxylate complex, offering abundant interactions with probes. Using two probes of FAM-ssDNA and triethylammonium salt (ROX)-ssDNA, the detection limits of DENV and ZIKV RNA sequences were 332 and 192 pmol/L for single fluorescence analysis, and 184 and 121 pmol/L for synchronous fluorescence analysis, respectively (3σ, where σ is the SD of a blank solution, $n = 3$). The detected time of both probes was 36 and 2 min, respectively. Both assays distinguished even single-base mismatched RNA sequences with high specificity. In contrast to single analysis, synchronous fluorescence analysis displayed enhanced sensing sensitivity and faster detection time, because it can avoid interference arising from Raleigh scattering light to the fluorescence sensing.

The abnormal expression of microRNA (miRNA) is exceedingly associated with the occurrence and development of diseases. qRT-PCR is the current gold standard clinical technology, [83] which possesses high sensitivity and specificity but suffers from insufficient simultaneous and multiple analysis methods for miRNAs at trace expression level. The ultrathin MOF nanosheets (MnDMS, $Mn(C_6H_8O_4)(H_2O)$) were prepared using manganese (Mn) ions and a flexible ligand of 2,2-dimethylsuccinate. [51] Most of the MnDMS nanosheets were nearly single layer by ultrasonication and Li-intercalation methods, and their thicknesses were calculated about 1 nm, showing the higher level of structural tailorability and good biocompatibility. The fluorescent sensing platform was combined with hybridization chain reaction (HCR), an enzyme-free amplification strategy, to significantly amplify the recovered fluorescence signal. The HCR/MnDMS system provided simple and sensitive determination of miRNA-21 with good linearity of 0.5 ~ 100 pmol/L. Interfering experiments indicated there was no interference in fluorescent sensing with interfering species as well as two and four-base mismatched sequences, showing its high sequence specificity in complex biosystems. This method also realized miRNA monitoring in living cells. Moreover, the determination of multiplex miRNAs could effectively improve the analysis efficiency for early disease detection and diagnosis. Qiu et al. reported a one dimensional (1D) water-stable MOF-based biosensor for the detection of gastric cancer associated with miRNAs (miR-185, miR-20a, miR-92b, miR-25, and miR-210). [63] The MOF of $\{[Cu(dcbb)_2(H_2O)_2]\cdot 10H_2O\}_n$ (**1**, H_2dcbbBr = 1-(3,5-dicarboxybenzyl)-4,4′-bipyridinium bromide) possessed aromatic rings, positively charged pyridinium, and uncoordinated carboxylates, which can effectively associate with five different FAM-ssDNA probes. The developed MOF showed good quenching ability for probes (QEs of 77 ~ 96%) via the PET mechanism. The detection limits of the miRNAs assay were between 91 and 559 pmol/L. Compared with other biosensors, this method achieved simple and multiplex detection of miRNAs only by selecting different complementary nucleic acid sequences, which also validated its appealing specificity and versatility. A novel sensing strategy was developed to detect multiplexed miRNAs in solution and living cancer cells. [35] As shown in Fig. 6a, the strategy was composed of nano MOF (UiO-66 of 125 nm particle diameter) and fluorophores-labeled peptide nucleic acid (PNA) probes. PNA, one of the most promising class of specific biological recognition molecules, is a synthetic DNA or RNA analogue whose phosphodiester backbone is replaced with unchanged 2-*N*-aminoethylglycine units. [84] Furthermore, it is resistant to enzymatic degradation by nucleases and proteases, and possesses higher specificity and stronger stability than DNA or RNA. The PNA-based probes were labeled with three different fluorophores, which were quenched by nano UiO-66

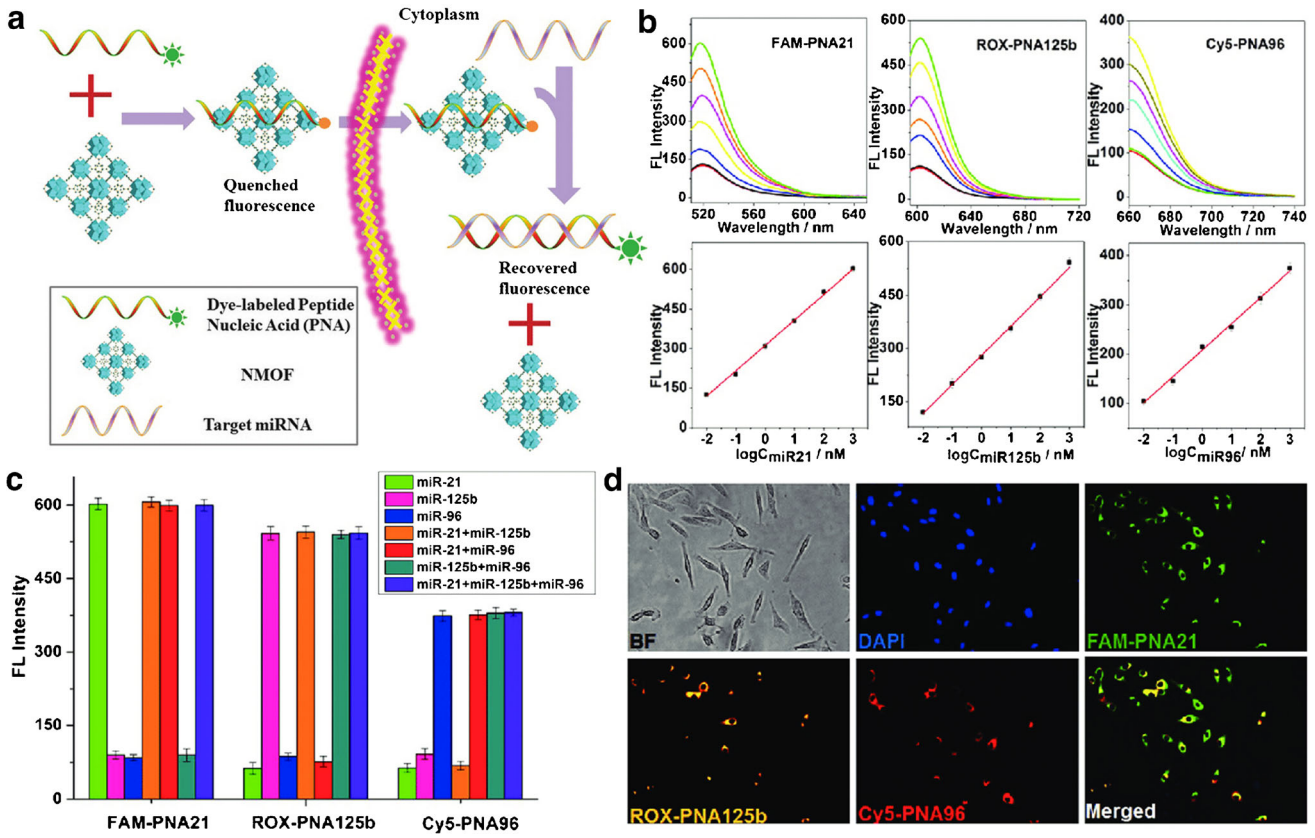

Fig. 6 UiO-66-based sensing strategies for multiplexed miRNAs detection [35]. Copyright 2015, Royal Society of Chemistry. **a** The PNA-MOF-based miRNA sensing mechanism. **b** Fluorescence spectra of three types of PNA-MOF complexes in response to different concentrations of miRNAs. **c** The sequence specificity and cross-reactivity of the proposed miRNA sensor. **d** Fluorescence images of MDA-MB-231 cells incubated with PNA-MOF complexes for 14 h

(QE of 81.6%) via the PET effect. In comparison to the above multiplexed assays, this biosensor displayed a wider linear range of 10 ~ 1000 pmol/L and lower detection limit of 10 pmol/L for miRNAs (miR-21, miR-96, and miR-125b). Besides, complementary miRNAs yielded about 5 ~ 8 times higher fluorescence recovery signals than non-complementary miRNAs (Fig. 6c), showing the high specificity and negligible cross-reactivity of this miRNA sensor. As shown in Fig. 6b–d, the biosensor not only allowed for quantitative and specific analysis of multiplexed miRNAs in solution, but also enabled precise monitoring of spatiotemporal changes of miRNAs expression in situ living cancer cells.

Proteins

Proteins are well known as vital working units for many life activities. The accurate quantitative analysis of abnormal protein expression is important in disease prevention and diagnosis. The determination strategies for disease-related proteins include enzyme-linked immunosorbent assay (ELISA), electrochemical immunoassay, and mass spectrometry, etc. [85] Many of these approaches are dependent on the immune responses between antigens and antibodies. Thus, operation of the assay is very cumbersome and expensive. Owing to the advantages of simplicity, rapidity, and low cost, the switch fluorescence biosensors using MOFs and nucleic acids were designed as new tools for the analysis of proteins.

A fluorescence biosensor for the determination of H_5N_1 antibodies was developed based on Cu(H_2dtoa) (H_2dtoa = *N*,*N*′-bis(2-hydroxyethyl)dithiooxamide) quenching toward FAM-DNA probes. [64] The 3′-terminus of the probes was modified with H_5N_1 antigens. After specifically binding with H_5N_1 antibody, it could inhibit the hydrolysis of exonuclease I (Exo I) to FAM-DNA probes. Therefore, the fluorescence of probes could not recover. Additionally, the presented biosensor refrained from DNA hybridization, simplifying the sensing process. It showed good sensitivity (1.6×10^{-9} mol/L, S/*N* = 3), detection range ($1 \times 10^{-9} \sim 1 \times 10^{-6}$ mol/L), and noteworthy selectivity, as well as satisfactory results for H_5N_1 antibody detection in serum samples. Compared with single-component MOFs, hybrid MOFs can provide more advantages of enhanced physicochemical and optical properties; Huang et al. proposed a "three-in-one" nanohybrid of Zr-MOF@AuNP@GO as the synergistic nanoquencher [41], which consisted of three common quenching nanomaterials (Fig. 7a–b). Zirconium (Zr)-based MOF (Zr-MOF), gold

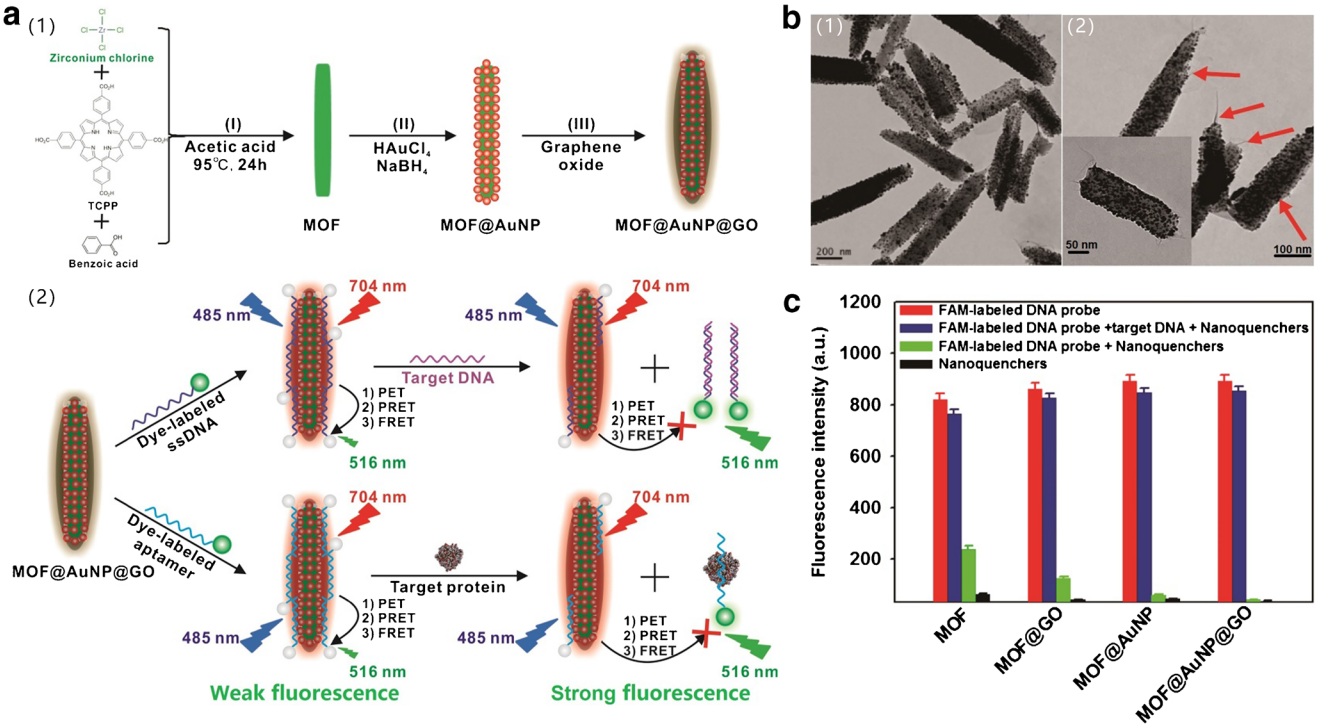

Fig. 7 The Zr-MOF@AuNP@GO-based biosensor for target DNA and protein detection [41]. Copyright 2018, Ivyspring International Publisher. **a** Schematic diagrams of (1) Zr-MOF@AuNP@GO synthesis and (2) detecting mechanism. **b** Transmission electron microscopy (TEM) images of Zr-MOF@AuNP@GO, in which the GO layer with filaments was indicated by the red arrows. **c** Fluorescence intensity under different experimental conditions: Zr-MOF, Zr-MOF@GO, Zr-MOF@AuNP, and Zr-MOF@AuNP@GO

nanoparticles (AuNPs), and graphene oxide (GO) significantly increased binding affinity to fluorophores labeled ssDNA and aptamer probes based on π-π stacking, van der Waals force, and hydrogen bonding. They quenched the fluorescence by PET, plasmonic resonance energy transfer (PRET), and FRET processes, respectively. Compared with MOF alone, the fluorescence quenching abilities of Zr-MOF@AuNP@GO nanohybrids were significantly enhanced within 5 min and almost QE of 100% (Fig. 7c). Using FAM-aptamer and FAM-ssDNA, a novel fluorescence biosensor was developed for rapid and sensitive detection of prostate specific antigen (PSA) and p53 gene in human serum. The linear detection ranges of 0.05 ~ 10 ng/mL and 0.01 ~ 10 nmol/L were attained for target protein and DNA, with detection limits as low as 0.01 ng/mL and 0.005 nmol/L ($S/N = 3$), and overall detection time of 35 and 10 min, respectively. For the specific determination of PSA, a signal increase was observed when PSA was presented in the serum sample, whereas there was no obvious change in the presence of other proteins in serum, indicating high selectivity against other interfering substances, such as human serum albumin, C-reaction protein, and alpha fetoprotein. Moreover, results of PSA-spiked human serum samples were highly accordant to that of a commercial ELISA kit method with the correlation coefficient (R^2) of 0.985, indicating its reliability in complex biological samples. These analytical behaviors were superior than most reported nanoquencher-based fluorescence biosensors due to lower background signal and higher S/N ratio.

A nanoscale MOFs (NMOFs)-based sensor array assembly fabricated with six specific biological recognition molecules was designed to effectively identify normal and pathological tissues, by making use of the different interactions between tumor marker proteins and DNA-adsorbed NMOFs. [86] As shown in Fig. 8a, three structurally stable NMOFs (Cu-MOFs, Fe-MOFs, and Zr-MOFs) featuring characteristic surface chemistry were utilized to adsorb two fluorophores labeled ssDNAs through π-π stacking, and then varying degrees of fluorescence quenching was achieved via the long-range energy transfer. The massive hydrophobic and hydrophilic patches on the surface of proteins allowed the protein analytes to interact with organic moieties or accessible coordination sites on NMOFs surface caused by intermolecular forces, including π-π stacking, coordination, hydrogen-bonding, and electrostatic interactions. These forces were considerably stronger than those of ssDNAs; thus, due to binding competition, ssDNAs could be displaced from NMOFs surface. These events caused variations in fluorescence intensity, providing a map of discriminative fingerprinting. Using linear discriminant analysis (LDA), the sensor array could rapidly (~1 h) identify tumorous tissues of colon cancer with high sensitivity

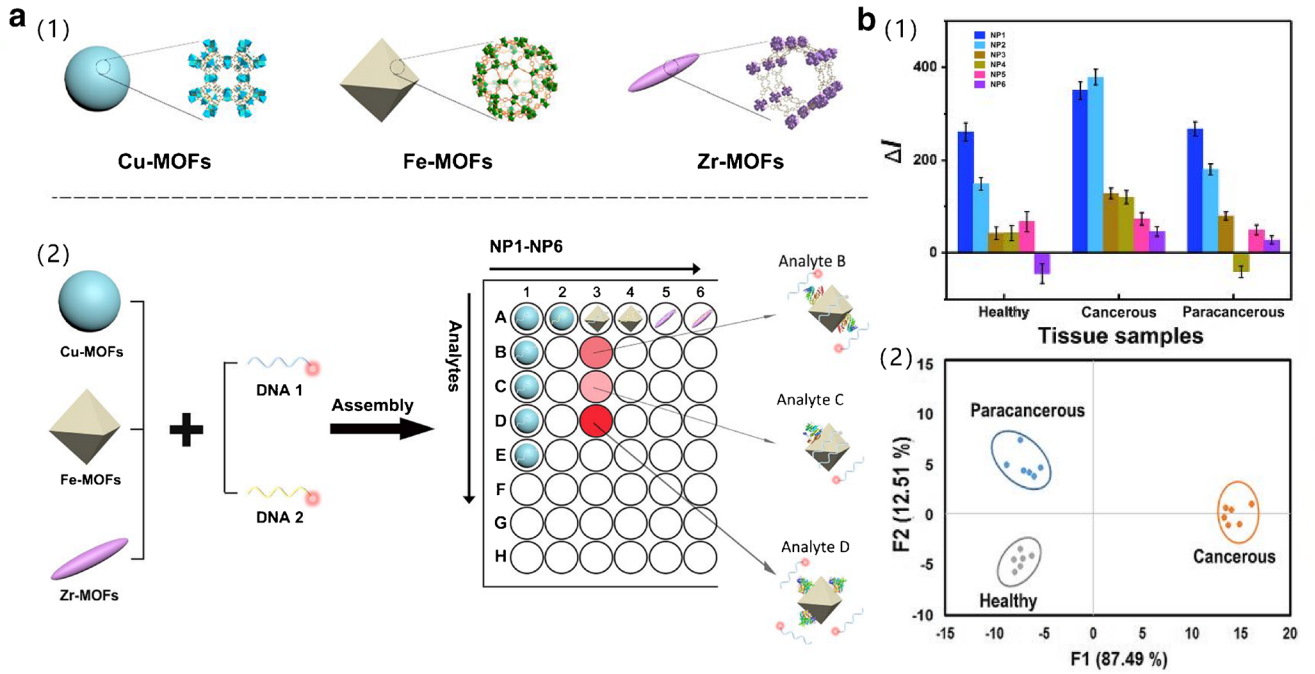

Fig. 8 A sensor array with NMOFs for the histopathological examination of colon cancer [86]. Copyright 2019, American Chemical Society. **a** Schematic illustration of sensing mechanism. (1) Three types of NMOFs. (2) Six specific biological recognition molecules designed by employing the nano-assembly between three types of NMOFs and two fluorophores labeled ssDNAs. The shades of the color represent fluorescence intensity. **b** Array-based sensing of tissue samples. (1) Fluorescence response (ΔI, I-I_0) patterns of the sensor array against various tissue samples: healthy, cancerous, and paracancerous ones with 150 ng. (2) Canonical score plot for the first two factors of fluorescence response patterns obtained from LDA analysis against three types of samples, with 95% confidence ellipses

and accuracy, enhancing diagnostic efficiency (Fig. 8b). Notably, different tissue samples of colon cancer were precisely differentiated at the 150-ng level, minimizing biopsy size. The unique design of their work was founded on the competitive interaction between ssDNA probes, proteins, and MOFs, shattering the traditional sensing pattern of specific biological recognition of protein targets and sensitive elements, and provided a novel biosensing strategy. However, only qualitative differentiation was realized, and could not achieve quantitative and precise analysis, which should be taken into consideration for their further studies.

Enzymes

Enzymes are vital biomolecules in all living organisms. The development of sensitive enzyme detection methods is vital for disease diagnosis and clinical research. Colorimetric methods have been principally used in clinical tests due to simplicity and low cost. [87] However, limitations do exist such as low sensitivity and vulnerability to interference. Therefore, fluorescent sensing assays are attractive alternatives because of high sensitivity and practicality. Recently, MOFs-based switch fluorescence biosensors were widely used for the detection of enzymes. The FAM-ssDNA and mixed valence state cerium (Ce^{3+}/Ce^{4+})-based MOF (MVCM) were employed as the signal unit and quenching nanoscaffold, respectively (Fig. 9a). [65] The MVCM was generated by the partial oxidation of a Ce^{3+}-based MOF precursor and showed a typical nanorod structure with an average length and width of 2.09 μm and 230 nm, respectively. In the presence of Ce^{4+}, QE of MVCM (> 90%) showed threefold increase compared to that of MOF, which only contained Ce^{3+}. The study verified that the quenching effect of MVCM to FAM-ssDNA could be blocked through competitive coordination between pyrophosphate ion (PPi) and binding sites (Ce^{3+} and Ce^{4+}) of MVCM. This displacement assay displayed high specificity to PPi (Fig. 9b). FAM-ssDNA was effectively displaced within 2 min from the surface of MVCM. Since PPi could undergo hydrolysis to phosphate ion by alkaline phosphatase (ALP), the PPi-triggered displacement method was further applied in ALP determination. As shown in Fig. 9c, because of the specific catalytic ability, only ALP suppressed the displacement of PPi and led to a remarkable change of FAM-ssDNA fluorescence, suggesting the highly specificity against foreign interferences. The method possessed a linear detection ranging from 2 to 100 mU/mL with a detection limit of 0.18 mU/mL ($S/N = 3$) (Fig. 9d). Additionally, the applicability of ALP determination was well approved in serum samples. The ALP recoveries of these spiked serum samples were from 95.65 to 100.60% and their RSDs ($n = 3$) were all less than 1.03%, which were in agreement with the results from the classic p-nitrophenyl phosphate

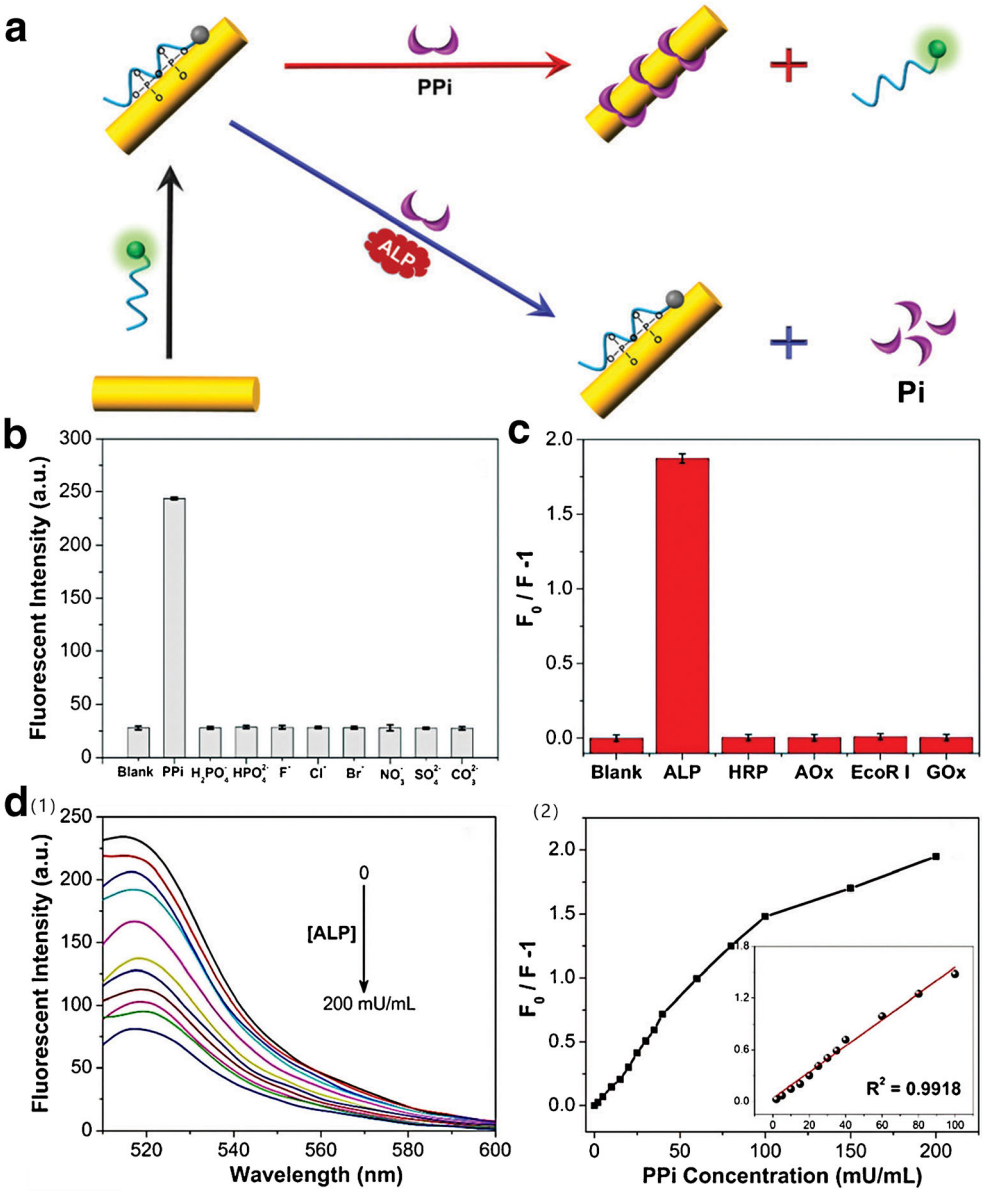

Fig. 9 PPi-triggered competitive displacement of ssDNA from a MOF and its application in fluorescent sensing of ALP [65]. Copyright 2018, Royal Society of Chemistry. **a** Schematic illustration of sensing process. **b** Fluorescent responses of the MVCM/FAM-ssDNA complex to PPi and various anions. **c** Fluorescent responses of the PPi-triggered sensing system to ALP and other enzymes. **d** Fluorescence spectra (1) and responses (2) of the PPi-triggered sensing system after the addition of ALP with different concentrations

colorimetric assay. The design of this proposed biosensor was very ingenious and unique, but there existed the restriction of other detecting targets, possibly limiting its wide application. Song et al. constructed a barium (Ba)-based coordination polymer of $[Ba_2(L)(H_2O)]\cdot(DMF)_{0.5}(H_2O)_3$ (H_4L = bis-(3,5-dicarboxy-phenyl)terephthalamide). This framework exhibited high stability up to 450 °C because of the strong barium-oxygen-barium linkages, and displayed the strong fluorescence quenching ability to FAM-ssDNA probes of different lengths. [46] Hence, a convenient and efficient analytical biosensor was developed for the activity assay of deoxyribonuclease I (DNase I) by taking the advantage of its catalytic ability to the decomposition of probes. A good linear relationship was observed in the range of 0.1 ~ 10 U/mL with a detection limit of 0.04 U/mL (S/N = 3). Its selectivity was well ensured depending on the high specificity of the enzymatic reaction. Additionally, excellent spiked recoveries in cell lysate were 98.0 ~ 102.7%, which satisfactorily confirmed the practical application of the assay. According to specific interaction between enzymes and substrates, another fluorescence biosensor was designed for matrix metalloproteinase-2 (MMP-2) determination based on the FRET process between $Cu(H_2dtoa)$ and semiconducting polymer dots (Pdots), which were made from conjugated polymer monomers. [43] In comparison with traditional organic dyes, the Pdots possessed the high fluorescence brightness and easy surface modification. The polypeptide chains ($COOH$-GHHYYGPLGVRGC-NH_2) were modified on Pdots surfaces as fluorescence probes,

containing the specific MMP-2 substrate domain (PLGVR) and π-rich motif (HHYY). With a 2D sheet structure, a large surface area, and conjugated π-electron system, Cu(H_2dtoa) could absorb polypeptide chains through π-π staking interactions and quench the fluorescence of Pdots (QE of 74.5%) via the FRET process. The recovered fluorescence intensity revealed a good linear relationship with MMP-2 concentrations in the range of 0.1 ~ 2.5 pg/mL. Due to the high specificity of the enzymatic cleavage, MMP-2 was quantificationally and accurately determined in the complex matrix, using some common metal ions, amino acids, and proteins as interferents.

Antibiotics

Antibiotics, as one of the most commonly used veterinary drugs, have been widely applied in animal production and the food industry, due to their low cost and tempting curative effect. However, the overuse of antibiotics obtained from food can cause accumulation in the human body, resulting in increased bacterial resistance and lesions of tissues and organs. [88] Various techniques, including high-performance liquid chromatography (HPLC), liquid chromatography-mass spectrometer (LC-MS), and gas chromatography-mass spectrometry (GC-MS), have been employed to determine antibiotic contaminants. [89] They demand professional technology, expensive equipment, and involve time-consuming procedures. The detection of antibiotic residues requires not only simple operation means, but also trace determination technologies with high sensitivity. Switch fluorescence biosensors based on MOFs and nucleic acids can fulfill the above requirements and have potential application prospects in the sensing of antibiotic residues.

Recently, our group used a highly stable zirconium-porphyrin MOF (PCN-222) as a fluorescence quencher to develop a rapid and ultrasensitive fluorescence biosensor for antibiotic detection [20] (Fig. 10a). PCN-222 was based on tetrakis(4-carboxyphenyl)porphyrin (H_2TCPP) ligands and Zr_6 clusters nodes, showing a rod-like shape and a micrometer-scale size. Because of π-conjugated H_2TCPP ligands and Zr ions with a high electron-accepting ability, the fluorescence of FAM-aptamer was quenched rapidly within 1 min at high quenching efficiency (QE > 95%), which was attributed to the combined effect of FRET and PET processes. Also, the H_2TCPP ligands can provide a stable emission fluorescence signal that remained unchanged with altering target concentrations. The detection sensitivity of this strategy was further enhanced via combination with ratiometric fluorescence signals derived from FAM-aptamer and H_2TCPP ligand. For example, the displayed biosensor for chloramphenicol (CAP) determination exhibited considerably lower detection limit of 0.08 pg/mL (three times the SD in the blank solution) and wider detection range of 0.1 ~ 1 × 10^4 pg/mL. The detection process was completed within about 26 min. The exceptional long-term sensing stability was demonstrated due to the strong Zr-O coordination bonds. Moreover, the existence of interference antibiotics did not cause the fluorescence recovery, indicating the aptamer endowed this biosensor with high specificity and negligible cross-reactivity. These observations suggested that the detection performance was superior to those reported for other material-based methods. This method was successfully applied to CAP determination in milk and shrimp samples. These spiked recoveries and RSDs (n = 3) were 89.91 ~ 106.15% and 4.73 ~ 8.51%, respectively, which were in good agreement with those of the commercial ELISA kit. Another hollow polydopamine (PDA)-based MOF (ZIF-67) acting as a fluorescent quencher, called metal-polydopamine framework (MPDA), was employed for dual detection of kanamycin (KANA) and oxyteracycline (OTC). [66] The high surface area of MPDA was polymerization of PDA owning plentiful functional groups, suitable for molecules determination. High sensitivity was achieved with detection limits of 304 pmol/L for KANA and 481 pmol/L for OTC, which were calculated by the 3σ method. Their sensitive and selective determination was also applied to milk samples with acceptable accuracy. Given that 2D MOFs with superior properties of inherent biodegradability and biological consistency can quench the most fluorophores, Yang et al. recently reported Cu-TCPP-based multicolor fluorescent aptamer nanoprobes for multiplexed antibiotic detection. [67] The platform utilized the double stirring bars assisted target replacement system with enzyme-free signal amplification. The sensing procedure is detailed in Fig. 10b, in which double stirring bars were decorated with AuNPs to increase specific surface area. The surface of bar 1 was coated with a branched DNA probe (Y-DNA), which was composed of fixed DNA (fDNA), assisted DNA (aDNA), and captured DNA (cDNA). Bar 2 was installed by ssDNA (fuel strand). When cDNA bound to targets, Y-DNA was disintegrated for target recycling. The cDNA/target complex could react with the fuel strand, and upon dsDNA formation, the target was released to carry out following reaction cycles. The aDNA in supernatant was also combined with a fluorescence signal probe (P), which was previously quenched by Cu-TCPP. Thus, the fluorescence intensity showed a remarkable enhancement after forming the dsDNA. The assay displayed sensitive determination of three antibiotic residues within 30 min, with LODs of CAP, OTC, and KANA being as low as 1.5, 2.4, and 1 pmol/L, respectively (S/N = 3). In comparison with nanomaterial-based fluorescence sensors, this universal platform for target multiple detection had higher sensitivity due to low background signals and enzyme-free amplification. The proposed biosensor showed a good anti-interference capability and high selectivity because of high affinities between targets and aptamers, although other interfering antibiotics, proteins, and metal ions were in existence. Moreover, it was preliminarily and satisfactorily applied for

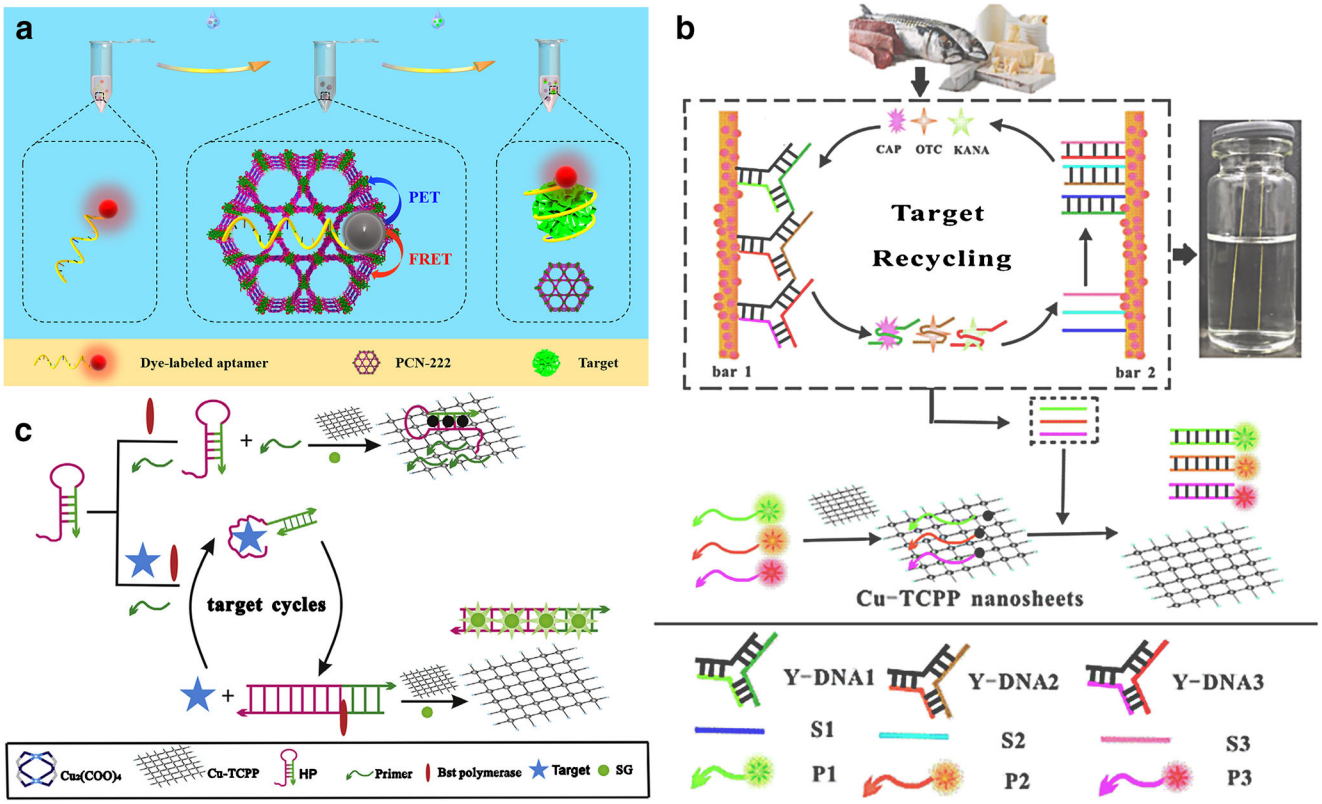

Fig. 10 Application of MOFs in food antibiotic detection. **a** Schematic illustration of the fluorescent assay with PCN-222 and dye-labeled aptamer as sensing platforms [20]. Copyright 2020, Elsevier. **b** Schematic representation of a multicolor fluorescence nanoprobe platform using Cu-TCPP nanosheets and double stirring bars assisted target replacement for multiple antibiotics [67]. Copyright 2019, American Chemical Society. **c** Schematic illustration of the Cu-TCPP nanosheets synthesis process and the detection of CAP based on CSRP target-triggered amplification strategy [44]. Copyright 2018, Elsevier

multicolor imaging of the aforementioned antibiotics in fish tissue slices.

The combination of MOF-based fluorescence quenching biosensors and enzyme-based amplification technologies can hugely improve the sensitivity of antibiotics determination. A FRET aptasensing platform was developed for CAP detection, employing Cu-TCPP nanosheets for quenching the background fluorescence and circular strand-replacement DNA polymerization (CSRP) for signal amplification. [44]. As shown in Fig. 10c, an aptamer hairpin probe (HP), whose stem was opened after binding to target, could bind with the primer. In the function of polymerase, an extension reaction was triggered to cause dsDNA, promoting release of the target for a new cycle. SYBR Green I (SG) could bind with dsDNA to generate strong fluorescence for quantification of target. The fluorescence of the HP/SG complex and free SG was quenched by Cu-TCPP nanosheets with QE of 85%, which did not influence the fluorescence of the dsDNA/SG complex resulting in negligible background signals. The results illustrated that the biosensor had a wide detection range of $1 \sim 1 \times 10^4$ pg/mL with detection limit of 0.3 pg/mL (S/N = 3) and determining time of 60 min. The high selectivity for the determination of CAP was well demonstrated when CAP and interfering substances were coexisted, for example, common antibiotics and proteins. Additionally, its good accuracy was also tested in several milk and fish samples. As such, He et al. selected MIL-101(Cr) to quench the fluorescence of FAM-aptamer, [39] and when it interacted with targets, DNA probes could depart from the surface of MIL-101(Cr), allowing fluorescence recovery. Then, they were hydrolyzed by RecJf exonuclease, in which the release targets triggered the next cycle, which promoted significant amplification of fluorescence signal. Furthermore, the selective and sensitive determination of OTC was possible based on this strategy. The linearity range was from 10 to 2×10^3 nmol/L, and detection limit was down to 4.2 nmol/L. Other antibiotics of high concentrations had no obvious interferences for OTC detection, whose high selectivity benefitted from the specificity of aptamers. The favorable applicability was verified in duck certified reference material.

Heavy metal ions

Contamination of heavy metal ions is a serious global problem due to high toxicity and non-biodegradable substances, as well as accumulation in the food chain and ultimately the human body. [90] Among the known toxic metals, mercury

ions (Hg^{2+}) are very deleterious to human health and the environment. Even at trace levels, Hg^{2+} ions can cause serious brain damage, kidney failure, and nervous disorder. [91] Therefore, the effective and sensitive detection of trace amounts of heavy metal ions is very important for health monitoring. Current quantitative approaches include atomic adsorption spectroscopy (AAS), atomic fluorescence spectroscopy (AFS), and inductively coupled plasma-mass spectroscopy (ICP-MS). [92] These classic methods possess reliable sensing performance and high sensitivity, but require expensive equipment and well-trained personnel, which limits their wide application in the field of rapid assay. To overcome these problems, MOFs and nucleic acids-based switch fluorescence biosensors are increasingly developed for the determination of heavy metal ions, owing to the very simple operation process and fast signal response.

Given that both of MOFs and PDA had excellent electron acceptors, integrating MOFs with PDA can further improve the quenching efficiency and enhance the sensitivity of fluorescence sensors. Ravikumar et al. proposed a PDA-coated ZIF-67 (MPDA) as strong fluorescence quencher for highly sensitive and selective determination of Hg^{2+} and Ag^{+} ions, which assisted through the exonuclease III (Exo III) signal amplification strategy [68] (Fig. 11a). The fluorescent QE toward fluorophores-labeled ssDNA was sufficient to achieve above 96% caused by FRET and PET processes. Based on T-Hg^{2+}-T and C-Ag^{+}-C base pairs, fluorophores-labeled ssDNA was self-hybridized to form dsDNA, which was separated from the MPDA surface, leading to fluorescence recovery. After the addition of Exo III, target recycling was achieved to enhance the sensitivity of fluorescence sensors efficiently. As shown in Fig. 11b, the detection ranges of Hg^{2+} and Ag^{+} were $1.3 \times 10^{-3} \sim 2$ nmol/L and $1 \sim 3$ nmol/L, and detection limits were 1.3×10^{-3} nmol/L and 3.4×10^{-2} nmol/L, respectively (3σ). Figure 11c showed that there were no significant fluorescence responses with the addition of interfering metal ions. The good specificity derived from the high affinity of T-Hg^{2+}-T and C-Ag^{+}-C mismatches for Hg^{2+} and Ag^{+}, respectively. The highly sensitive determination of tap water and river water samples was further evaluated with satisfactory recovery results, showing the potential application of the biosensor for the determination of trace amount of Hg^{2+} and Ag^{+}. Recently, based on the magnetic and adsorption properties of magnetic nanoparticles (Fe_3O_4), Marieeswaran et al. designed and synthesized a magnetic nanoscale MOF (NH_2-MIL-101(Fe)@Fe_3O_4), which adsorbed FAM-ssDNA on the surface via π-π stacking interactions and partly quenched its fluorescence. [69] The introduction of Hg^{2+} ions produced dsDNA and further enhanced fluorescence quenching. Uncoordinated Fe^{3+} ions on the MOF surface resulted in re-adsorption of dsDNA, thus showing a drastic decrease in fluorescence intensity with Hg^{2+}. The biosensor's detection limit was 8 nmol/L (3σ) with good selectivity. Additionally, a 3D gadolinium (Gd)-based coordination polymer was developed for Hg^{2+} ions detection, where this crystal structure displayed the high thermal stability up to 400 °C and the water stability in a wide pH range (pH $2 \sim 10$). [93] The fluorescence intensity of FAM-ssDNA was quenched up to about 91% within 15 min. The recovered fluorescence intensity depended on Hg^{2+} concentrations and had an excellent selective property for Hg^{2+} sensing.

In addition to sensing a single heavy metal, several biosensors were also explored for the successive detection of Hg^{2+} ions and other pollutants by Chen's group. The prepared biosensor was employed for successive sensing of Hg^{2+} and I^{-}, which was composed of FAM-ssDNA and 2D MOF of $\{[Cu(Dcbb)(Bpe)]\cdot Cl\}_n$ (**1**, $H_2DcbbBr$ = 1-(3,5-dicarboxybenzyl)-4,4′-bipyridinium bromide, Bpe = *trans*-1,2-bis(4-pyridyl)ethylene)). [94] The MOF **1** resulted in fluorescence quenching through the PET process, and QE was 90.5%. The dsDNA comprising hairpin-like T-Hg^{2+}-T composition (dsDNA@Hg^{2+}) was given after capturing Hg^{2+}. Upon further addition of I^{-} into the system, Hg^{2+} was extracted from the dsDNA@Hg^{2+} duplex, due to stronger Hg-I coordination. The released FAM-ssDNA was resorbed to accompany the fluorescence quenching again. Consequently, this switch fluorescence sensor sequentially determined Hg^{2+} and I^{-} with high sensitivity and specificity. Their detection limits were calculated as 3.2 and 3.3 nmol/L, respectively, which were based on the 3σ/slope (σ = SD for 10 blank samples). Similarly, 3D MOF of $\{[Cu(Cdcbp)(bipy)]\cdot 4H_2O\}_n$ (**1**, $H_3CdcbpBr$ = 3-carboxyl-(3,5-dicarboxybenzyl)-pyridinium bromide; bipy = 4,4′-bipyridine) was applied to Hg^{2+} and biothiols. [95] Subsequent introduction of biothiols further competitively combined Hg^{2+} from the dsDNA@Hg^{2+} duplex driven by the stronger affinity between Hg^{2+} and biothiols, thus releasing FAM-ssDNA into the next round. According to the 3σ/slope (σ = SD of five 11 blank measurements), the detection limits of Hg^{2+} and biothiols toward cysteine (Cys), glutathione (GSH), and homocysteine (Hcy) were calculated as 3.0, 14.2, 15.1, and 8.0 nmol/L, respectively. Furthermore, the sensing mechanism was validated via experimental and theoretical analysis. On the basis of this sensing scenario, this group also reported a 1D MOF of $[Cu(Cdcbp)(H_2O)_2\cdot 2H_2O]_n$ for rapid sequential determination of Hg^{2+} and abovementioned biothiols, with detection limits of 2.3, 29.6, 19.8, and 10.2 nmol/L, respectively (3σ/slope, σ = SD of five blank measurements). [96] All above methods employed the competitive combination of Hg^{2+} and target to complete successive detection, which simplified time-consuming operation steps. However, the occurrence of their competitive combination was dependent on the affinity among Hg^{2+}, target, and MOF. Therefore, insufficient specificity toward the latter target was a bottle-neck to explore successive assays for highly efficient sensing, which hindered the scope of practical application. Consequently, horseradish peroxidase (HRP) was

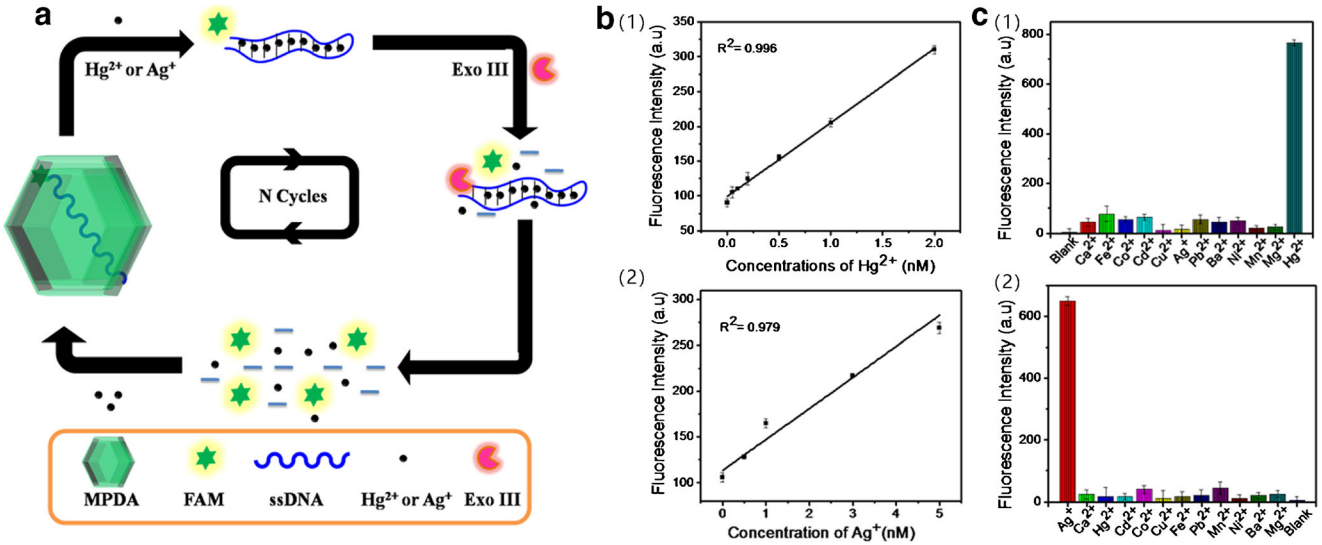

Fig. 11 Metal-polydopamine framework (MPDA)-based fluorescent sensing system for the determination of Hg^{2+} and Ag^{+} through Exo III signal amplification activity [68]. Copyright 2018, American Chemical Society. **a** Schematic illustration of the sensing strategy. **b** Linear relationship between the fluorescence intensity and concentrations of Hg^{2+} (1) and Ag^{+} (2). **c** Fluorescence intensity of different metal ions with Hg^{2+} (1) and Ag^{+} (2)

encapsulated into ZIF-8 (HRP@ZIF-8) by a biomimetic mineralization approach, in which, irregular sphere structures were obtained with average sizes of 520 ± 2.9 nm. [97] The HRP@ZIF-8 biocomposite significantly enhanced the tolerance to alkaline environments and high temperatures and also exhibited long-term stability. Most importantly, the biocomposite acted as fluorescence quencher and active biocatalyst was employed to the construction of HRP@ZIF-8/DNA hybrids. They were successively utilized as a fluorescent and colorimetric biosensor, and easily achieved successive detection of Hg^{2+} and phenol (Fig. 12a). Upon addition of FAM-ssDNA, the hybrid system achieved sensitive fluorescence determination of Hg^{2+} in concentration range of 0.22 ~ 2 nmol/L with a detection limit as low as 0.22 nmol/L (Fig. 12c). Subsequently, harnessing the excellent catalytic activity of HRP@ZIF-8 biocomposite allowed the development of a facile and sensitive colorimetric sensor for phenol detection, which gave a quantitative determination range of 0.5 ~ 100 μmol/L with corresponding detection limit down to 0.5 μmol/L (Fig. 12d). As shown in Fig. 12b, HRP@ZIF-8 biocomposite appeared much clearer and with denser color changes than that of free HRP in the phenol concentration range of 0 ~ 300 μmol/L. More interestingly, this naked-eye visualization mode yielded satisfactory specificity and sensitivity (0.7 μmol/L). The proposed system possessed high selectivity and excellent sensitivity toward Hg^{2+} (Fig. 12e) and phenol (Fig. 12f), respectively. This work well broadened up the potential of MOFs for successive determination of multiple pollutants.

Other analytes

A selection of novel switch fluorescence biosensors using MOFs and nucleic acids were developed to determine amino acid and organic compound. A rapid and facile sensing platform based on 2D Cu-MOF of $[Cu(mal)(bpy)]\cdot 2H_2O$ (mal = DL-malic acid, bpy = 4,4′-bipyridyl) was developed for the detection of specific small-sized amino acids. [70] The Cu-MOF could adsorb and quench fluorophore-ssDNA, following the static quenching mechanism with QE of 91.4%. Specific small-sized amino acids (for example glycine and serine) owning carboxyl and amino groups had a strong coordination ability, and then replaced the ligands of Cu-MOF probably due to the strong coordination of the hydroxyl group with Cu-MOF. This encouraged destruction of MOFs, resulting in recovery of the fluorescence of fluorophore-ssDNA. The results demonstrated that the concentration ranges for glycine (Gly) and serine (Ser) determination were 0.81 ~ 100 μg/mL (10.8 ~ 1.3 × 10^3 μmol/L) and 5 ~ 500 μg/mL (50 ~ 4.76 × 10^3 μmol/L), in which the detection limits were 0.81 μg/mL (10.8 μmol/L) and 1.51 μg/mL (14.4 μmol/L), respectively (S/*N* = 3). Except biosensing applications in real serum samples, this strategy was also employed for the construction of OR biomolecular logic gate based on glycine and DNA strand as inputs, which greatly enriched the building blocks of DNA molecular logic gate. Another nano-sized Fe-MIL-88B-NH_2-based fluorescent biosensor was developed for the detection of bisphenol A (BPA). [71] The determination range was between 5.0 × 10^{-14} and 2.0 × 10^{-9} mol/L, generating a detection limit of 4.1 × 10^{-14} mol/L (S/N = 3).

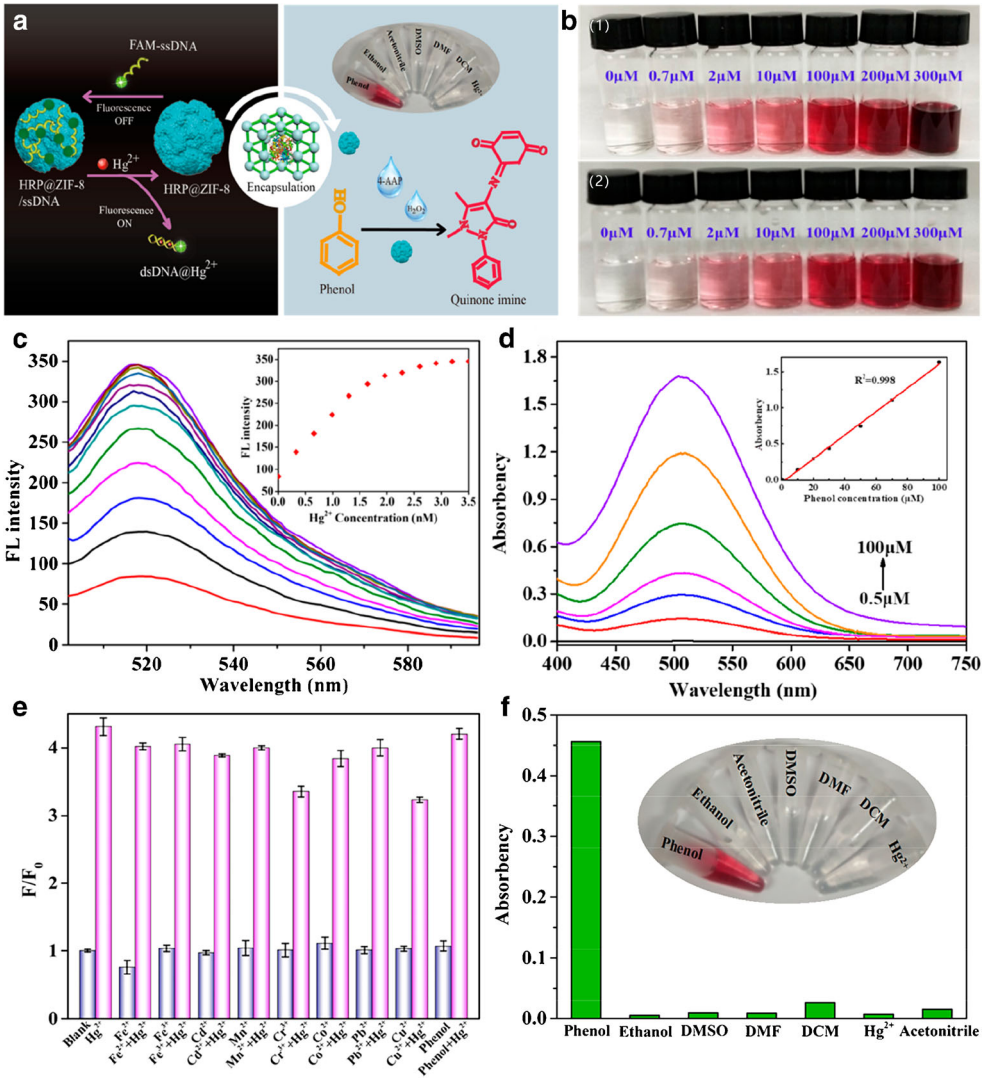

Fig. 12 HRP@ZIF-8/DNA hybrids for successive determination of Hg^{2+} and phenol [97]. Copyright 2019, American Chemical Society. **a** Schematic illustration of the biosensor. **b** Naked-eye detection of phenol by using HRP@ZIF-8 (1) and free HRP (2). **c** Fluorescence spectra of Hg^{2+} biosensor with various concentrations of Hg^{2+}, and corresponding fluorescence intensity plotted against Hg^{2+} concentration (inset). **d** UV-vis absorption spectra of HRP@ZIF-8 solution upon progressive adding of phenol, and calibration curve of absorbance at 505 nm versus phenol concentration (inset). **e** Selectivity of the Hg^{2+} biosensor against other metals. **f** Selectivity of the phenol biosensor against various analytes

Integrated MOF materials, with each material keeping its own identity, have been also developed for the analysis of adenosine triphosphate (ATP) and biotoxin. Considering the favorable easy-functionalization, biocompatibility, and high fluorescence QE, polydopamine (PDA) was usually functionalized on the surfaces of materials. Xu et al. reported a novel and sensitive fluorescent biosensor applying PDA-coated Zr-MOF (PDA/UiO-66) for ATP determination. [37] PDA/UiO-66 nanoparticles protected FAM-aptamers adsorbed on their surfaces from DNase I cleavage, allowing fluorescence quenching (QE of 99.1%). After binding with ATP, the complexes between FAM-aptamer and ATP were desorbed from nanoparticles and digested by DNase I. The released ATP could combine with other aptamer on PDA/UiO-66 to restart a new cycle. The recovering fluorescence intensity showed a linear relationship over a low ATP concentration range of 35 ~ 1×10^3 nmol/L. Its detection limit was calculated to be 35 nmol/L at the 3σ method, which was 5.7-fold higher than 200 nmol/L using the UiO-66-based method. There was only response to ATP in this system, choosing three interfering analogs (guanidine, cytosine, and uridine triphosphate). The efficient and sensitive detection of ATP was realized by this DNase I-assisted recycle amplification strategy. By employing the universal design concept of switch fluorescence biosensing, a nanocomposite of Fe_3O_4/g-C_3N_4/HKUST-1 was synthesized for the determination of ochratoxin A (OTA) in corn samples. [45] HKUST-1 was made up of copper nodes with 1,3,5-benzenetricarboxylic acid (H_3BTC) ligands, which was a kind of classical MOF defined by the Hong Kong University of Science and Technology. In the nanocomposite, the introduction of Fe_3O_4 and g-C_3N_4 (graphitic-phase carbon nitride) was aimed to reduce the background of the sensors by magnet separate, and improve its chemical stability and quenching capacity of HKUST-1, respectively. The composite possessed strong adsorption ability for FAM-aptamer and completely underwent fluorescence

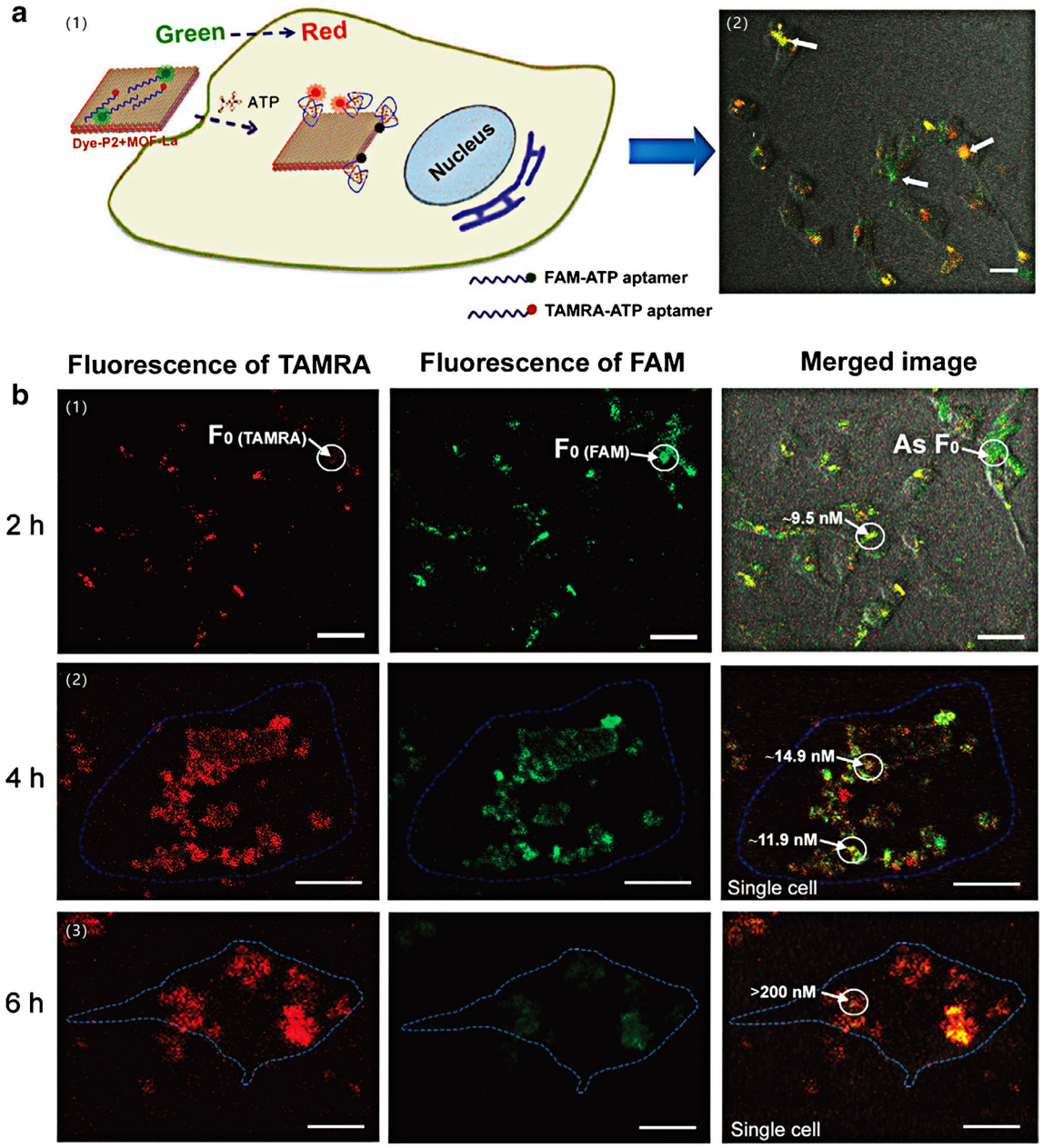

Fig. 13 Lanthanide-based MOF nanosheets for two-color intracellular ATP imaging in living cells [100]. Copyright 2017, Springer Nature. **a** Intracellular fluorescent imaging of ATP: (1) Schematic illustration of intracellular ATP probing in living cells using dye-aptamer+MOF-Ln, (2) Monitoring of ATP in living cells. **b** Confocal images of intracellular visualization for ATP with an incubation time of 2 to 6 h (1–3) and semi-quantification of ATP by two-color fluorescence

quenching by the PET mechanism. OTA concentration was in the range of 5 ~ 160 ng/mL, and detection limit was 2.57 ng/mL ($S/N = 3$) with good selectivity and repeatability.

Bioimaging of intracellular analytes

Intracellular analytes are the fundamental components of life activities, which can provide more real-time information to evaluate the occurrence, development, and prognosis of diseases. Therefore, it is of great significance to develop precise quantifiable and imaging methods for intracellular analytes. The existing assays include well-established fluorescence spectroscopy, Raman spectroscopy, and their imaging technologies. Raman spectroscopy contributed sensitive and noninvasive fingerprint information for analytes. However, its signal intensity was largely dependent on the surface plasmon resonance (SPR)-based enhancement effect of the plasmonic nanomaterials, such as silver and gold nanostructures. [98] Thus, Raman-based spectroscopy possessed distinct

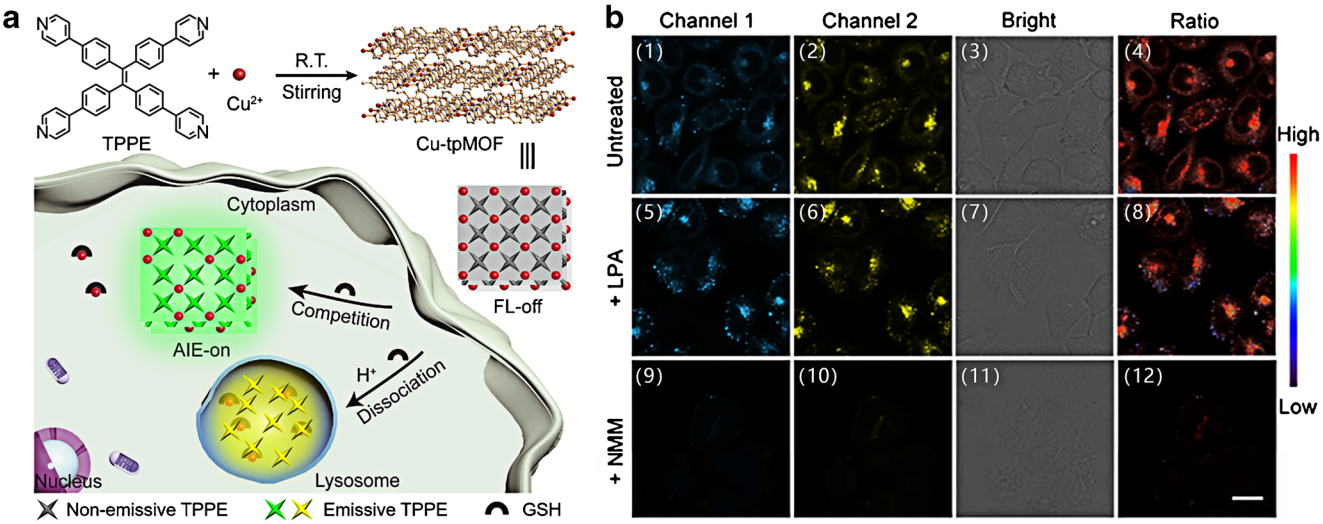

Fig. 14 Quencher-delocalized emission strategy of AIEgen-based MOF for profiling of subcellular GSH [101]. Copyright 2019, John Wiley and Sons. **a** Schematic illustration of the synthesis and quencher-delocalized emission strategy of Cu-tpMOF in living cells for profiling of GSH. **b** Confocal fluorescence images of HepG2 cells treated with α-lipoic acid (LPA) and N-methylmaleimide (NMM) from channel 1 collected at 460 ~ 480 nm (1, 5, 9), channel 2 collected at 600 ~ 620 nm (2, 6, 10), bright field (3, 7, 11), and ratio images of Channel 2/1 (4, 8, 12) under excitation at 405 nm

challenges such as time-consuming and expensive detection. Whereas, fluorescence spectroscopy is still a valuable tool for the exploration of intracellular analytes, owing to their attractive advantages of sensitivity, simplicity, and signal stability. [99] In combination with MOFs and biosensing elements, fluorescence-based techniques display potential applications in the bioimaging of intracellular analytes, including cellular ATP, subcellular GSH, and cellular membrane protein.

Owing to the good biodegradable characteristics and structural tailorability of nano-scaled MOFs, a series of novel lanthanide-based MOF (MOF-Ln) nanosheets were prepared as fluorophore-labeled aptamer platform using the ligand of 2,2′-thiodiacetic acid ($S(CH_2COO)_2^{2-}$, TDA) [100], in which, Ln were La, Nd, europium (Eu), Tb, and erbium (Er). This prepared MOF-La structure was a crystalline nanosheet with an ultrathin thickness of 2.0 nm, the size of most of that was smaller than 500 × 500 nm. After quenching on MOF-Ln nanosheets, the fluorescence response was associated with the charge properties of fluorophores. Upon interacting with target biomolecules, negatively charged fluorophores (FAM) generated a further "turn-down" fluorescence response, whereas the positively charged fluorophores (TAMRA) showed a "turn-up" process. Adjustment of the molecular ratio of TAMRA to FAM allowed the design of two-color nanoprobes of fluorophore-aptamer/MOF-Ln nanosheets for assaying ATP activity. They showed a linear range of 0.5 ~ 15 nmol/L and low detection limit of 500 pmol/L. This biosensor also had good selectivity toward ATP and other biomolecules in real samples, such as human plasma and cell extracts. More importantly, based on the stable dispersion of MOF-Ln in the biosystem, the biosensor was successfully employed to monitor ATP activity in living cells. As shown in Fig. 13a, after 4 h incubation time, the sensitive fluorescence color change was observed from green to red in different cells. As seen in Fig. 13b, with the increase in incubation time, the difference in fluorescence color was also clearly visible in different regions of a single cell. Moreover, the ATP concentration in living cells can be semi-determined by calculating the ratio of TAMRA to FAM. Compared with traditional fluorescence biosensors, this two-color sensing platform effectively avoided interference from false-positive observations, and veritably revealed the distribution of biomolecules in living cells.

In addition to the use of fluorophore-based probes for biomedical imaging, a quencher-delocalized emission strategy was reported for in situ profiling of glutathione (GSH) at different subcellular locations in living cells [101]. The study showed the design of non-emissive MOF nanoprobe (Cu-tpMOF) using Cu^{2+} as the node and quencher tetra(4-pyridylphenyl)ethylene (TPPE) as the ligand, producing an iconic aggregation-induced emission (AIEgen). The size of as-synthesized Cu-tpMOF was around 100 nm, and it revealed the good biocompatibility. As shown in Fig. 14a, the Cu^{2+}-induced electron transfer process could quench the fluorescence of the AIEgen-based Cu-tpMOF structure. The Cu^{2+} in MOF was competed by GSH in a neutral environment (cytoplasm) to partially delocalize Cu^{2+}, emerging green fluorescence. Then, MOF was completely dissociated to generate yellow fluorescence under acidic environment (lysosome), owing to binding between GSH and Cu^{2+} as well as protonation of TPPE. To simultaneously profile GSH in both cytoplasm and lysosomes, a two-channel fluorescence imaging strategy was developed based on collecting green fluorescence (channel 1) and yellow fluorescence (channel 2). As

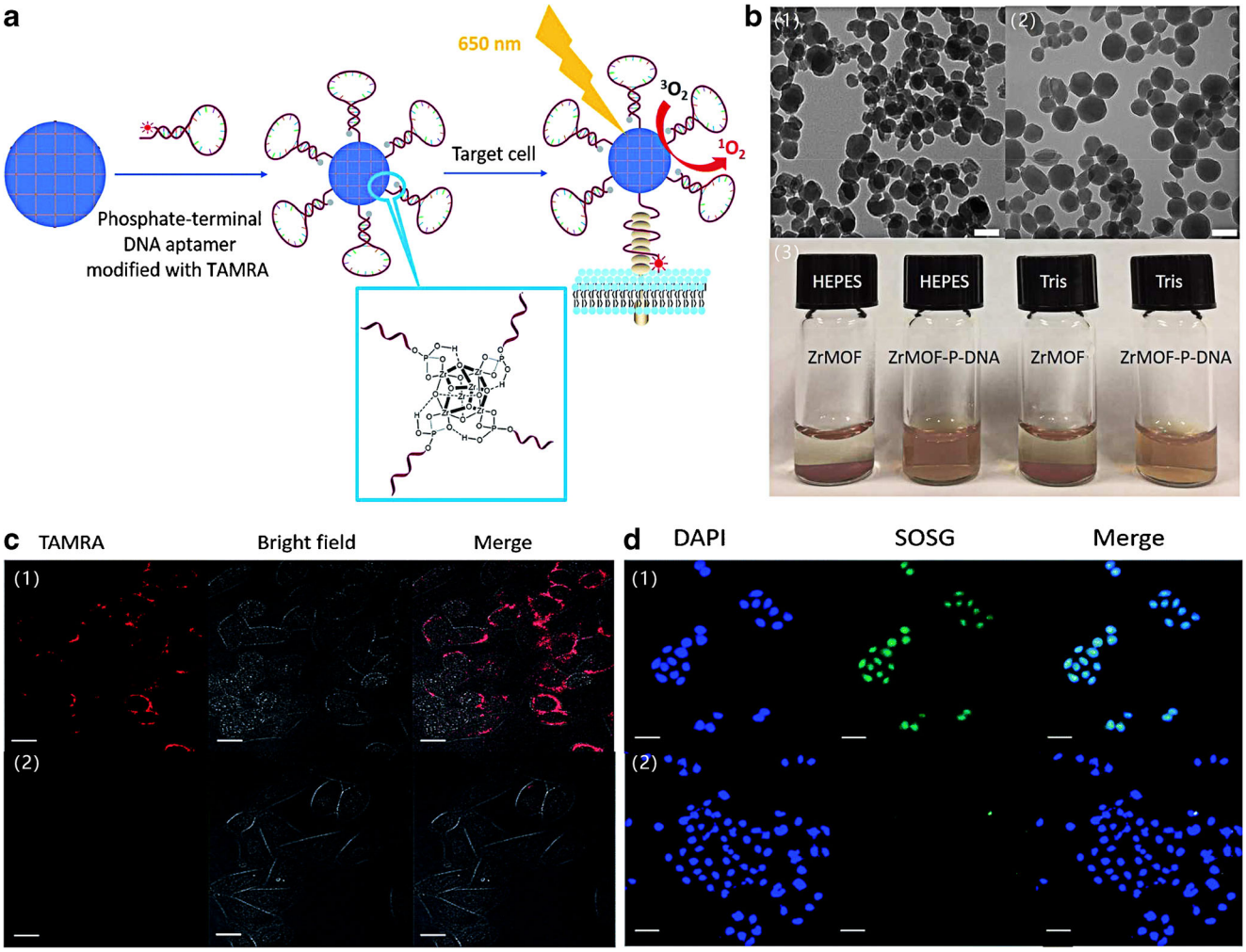

Fig. 15 Porphyrinic Zr-MOF nanoparticles as quencher to conjugate DNA aptamer for target-induced bioimaging and photodynamic therapy [102]. Copyright 2019, Royal Society of Chemistry. **a** Schematic illustration of phosphate-terminal DNA aptamer conjugation to Zr-MOF nanoparticle quencher for target-induced imaging and photodynamic therapy. **b** TEM images of synthesized Zr-MOF nanoparticles in DMF (1) and aptamer-conjugated Zr-MOF nanoparticles (Zr-MOF-P-aptamer) in water (2); (3) Stability test of Zr-MOF and Zr-MOF-P-aptamer nanoparticles in HEPES and Tris buffers, respectively. **c** Positive (1) and negative (2) confocal imaging of HeLa cells incubated with Zr-MOF-aptamer-TAMRA and Zr-MOF-Library-TAMRA, respectively. **d** Singlet oxygen detection right after treatment: positive (1) and negative group (2)

shown in Fig. 14b (1) and (2), after endocytosis, different patterns of fluorescence intensities of Cu-tpMOF were observed in both channels 1 and 2. From the ratio image of channel 2-to-1 signals in Fig. 14b (4), the area with pseudo red color (high channel 2-to-1 ratio) indicated GSH in acidic environment, while the pseudo blue color (low channel 2-to-1 ratio) suggested GSH in higher pH environment. The observations demonstrated that Cu-tpMOF was distributed in the cytoplasm and lysosome. The AIEgen-based MOF allowed for two-channel ratiometric analysis of dual-colored emissions, promoting real-time visualization of subcellular GSH in living cells. Meanwhile, this strategy was further utilized to survey drug effects on dynamic subcellular GSH perturbation.

Porphyrinic Zr-MOF nanoparticles as quencher to conjugate aptamer were developed for target-induced bioimaging and photodynamic therapy. [102] The Zr-MOF nanoparticles were synthesized using zirconyl chloride ($ZrOCl_2$) and the porphyrinic organic linker of tetra(4-carboxyphenyl) porphine (TCPP), and their size was around 110 nm. Usually, the cellular uptake of the MOF nanoparticles was through endocytosis, with respect to their size, shape, and surface chemistry. [103] By conjugating nanoparticles with specific biological recognition molecules, such as aptamers, antibodies, and peptides, the nanoparticles can bind with cell-surface receptors and enter cells through receptor-mediated endocytosis. [103, 104] Therefore, the cellular uptake into cancer cells was effectively enhanced and the target binding ability was greatly improved. In this work, a phosphate-terminal DNA aptamer was anchored on the surface of Zr-MOF nanoparticles by the strong coordination between phosphate and zirconium

(Fig. 15a). Surprisingly, this conjugation of aptamers dramatically improved the biostability of Zr-MOF nanoparticles in hydroxyethylpiperazine ethane sulfonic acid (HEPES) and tris(hydroxymethyl)aminomethane (Tris) buffers. As shown in Fig. 15b, aptamer-conjugated Zr-MOF nanoparticles revealed much better stability after 24 h than unmodified Zr-MOF nanoparticles, showing their potential for biomedical applications. The selected Sgc8 aptamer can bind the target cellular membrane protein PTK7 expressed on HeLa cells. Given that Zr-MOF nanoparticles promoted FRET-induced quenching of TAMRA-aptamer, target-induced imaging was achieved upon binding with the target (Fig. 15c). Except for biomedical imaging, porphyrinic MOF nanoparticles were applied for photodynamic therapy of cancer (Fig. 15d). Their periodic porous structure could availably address some defects of traditional photosensitizer such as poor solubility, self-quenching, and aggregation, [105] and enhance diffusion efficiency of cytotoxic reactive oxygen species (ROS). Moreover, the good biocompatibility and high selectivity of aptamer-conjugated Zr-MOF nanoparticles toward malignant tissues also significantly enhanced photodynamic therapy, making them promising candidates for the application of biochemistry.

Conclusions and perspectives

Herein, we have summarized recently reported applications of MOFs and nucleic acids-based switch fluorescent biosensors in the in vitro detection of different types of analytes and the bioimaging of intracellular analytes. The MOFs sensing field has undergone continuing growth especially over the past decade, showing increasing potential. Compared with other classical fluorescence quenching materials, such as activated graphene and quantum dots, MOFs have the following outstanding advantages in biosensors. [106–108] (1) The structure is clear, well-organized, flexible, and diverse, which is achieved via tuning metal ions, organic ligands or reaction conditions, various structures with different physiochemical properties, shapes, and sizes. (2) It has high specific surface area, porosity, and a tunable porous structure, which is beneficial to interactions among materials, biomolecules, and analytes. (3) The metal ions and organic ligands contain abundant active sites that are easily functionalized, which can combine different biomolecules or modify specific functional groups to satisfy the realistic sensing requirements.

Although the switch fluorescence biosensors based on MOFs and nucleic acids have received wide applications in detecting field, some challenges remain. (1) Fluorescence quenching mechanisms of MOFs have been studied in literatures, but the relevant mechanism research would not be comprehensive and systematic, and requires further attention. (2) The fluorescence quenching efficiency of some MOFs is insufficient, such as UiO-66 and ZIF-8, which decreases the detection sensitivity, and extends analysis time. The detection performances can be improved by the combination of signal amplification technique and other quenching materials. (3) The MOFs in the detecting systems cannot be reused, which reduces cost-effectiveness. The separation and reusing effects can be obtained through the combination of MOFs with magnetic materials. Thus, MOFs can be integrated with other functional materials to form composites, allowing a synergistic enhancement effect of both components, which is beneficial to the improvement of the material performance and can realize the effect of $1 + 1 > 2$. Furthermore, there are a great variety of MOFs types and selections of its complex materials are considerably more, thus providing composites with abundant properties and functions. It can be expected that under the joint efforts of numerous scientific researchers, the switch fluorescence biosensing technology based on MOFs and nucleic acids will embody broader application prospects in the future.

Acknowledgements This work was supported by the National Key Research and Development Program of China (No. 2018YFC1602903, 2018YFC1602904) and the National Natural Science Foundation of China (No.21976210).

Compliance with ethical standards

Conflict of interest The authors declare that they have no conflict of interest.

References

1. Yang Q, Xu Q, Jiang HL (2017) Metal-organic frameworks meet metal nanoparticles: synergistic effect for enhanced catalysis. Chem Soc Rev 46(15):4774–4808. https://doi.org/10.1039/c6cs00724d
2. Eddaoudi M, Kim J, Rosi N, Vodak D, Wachter J, O'Keeffe F, Yaghi OM (2002) Systematic design of pore size and functionality in isoreticular MOFs and their application in methane storage. Science 295(5554):469–472. https://doi.org/10.1126/science.1067208
3. Wang B, Cote AP, Furukawa H, O'Keeffe M, Yaghi OM (2008) Colossal cages in zeolitic imidazolate frameworks as selective carbon dioxide reservoirs. Nature 453(7192):207–211. https://doi.org/10.1038/nature06900
4. Latroche M, Surble S, Serre C, Mellot-Draznieks C, Llewellyn PL, Lee JH, Chang JS, Jhung SH, Ferey G (2006) Hydrogen storage in the giant-pore metal-organic frameworks MIL-100 and MIL-101. Angew Chem Int Ed Engl 45(48):8227–8231. https://doi.org/10.1002/anie.200600105
5. Ma S, Sun D, Simmons JM, Collier CD, Yuan DQ, Zhou HC (2008) Metal-organic framework from an anthracene derivative containing nanoscopic cages exhibiting high methane uptake. J Am Chem Soc 130(3):1012–1016. https://doi.org/10.1021/ja0771639
6. Cavka JH, Jakobsen S, Olsbye U, Guillou N, Lamberti C, Bordiga S, Lillerud KP (2008) A new zirconium inorganic building brick forming metal organic frameworks with exceptional stability. J

Am Chem Soc 130(42):13850–13851. https://doi.org/10.1021/ja8057953
7. Jiao L, Seow JYR, Skinner WS, Wang ZU, Jiang HL (2019) Metal-organic frameworks: structures and functional applications. Mater Today 27:43–68. https://doi.org/10.1016/j.mattod.2018.10.038
8. Xia W, Mahmood A, Zou R, Xu Q (2015) Metal-organic frameworks and their derived nanostructures for electrochemical energy storage and conversion. Energy Environ Sci 8(7):1837–1866. https://doi.org/10.1039/c5ee00762c
9. Rodenas T, Luz I, Prieto G, Seoane B, Miro H, Corma A, Kapteijn F, Llabres IXFX, Gascon J (2015) Metal-organic framework nanosheets in polymer composite materials for gas separation. Nat Mater 14(1):48–55. https://doi.org/10.1038/nmat4113
10. Huang YB, Liang J, Wang XS, Cao R (2017) Multifunctional metal-organic framework catalysts: synergistic catalysis and tandem reactions. Chem Soc Rev 46(1):126–157. https://doi.org/10.1039/c6cs00250a
11. Zhang K, Meng X, Cao Y, Yang Z, Dong H, Zhang Y, Lu H, Shi Z, Zhang X (2018) Metal-organic framework nanoshuttle for synergistic photodynamic and low-temperature photothermal therapy. Adv Funct Mater 28(42). https://doi.org/10.1002/adfm.201804634
12. Duan Y, Ye F, Huang Y, Qin Y, He C, Zhao S (2018) One-pot synthesis of a metal-organic framework-based drug carrier for intelligent glucose-responsive insulin delivery. Chem Commun 54(42):5377–5380. https://doi.org/10.1039/c8cc02708k
13. Lian X, Huang Y, Zhu Y, Fang Y, Zhao R, Joseph E, Li J, Pellois JP, Zhou HC (2018) Enzyme-MOF nanoreactor activates nontoxic paracetamol for cancer therapy. Angew Chem Int Ed Engl 57(20):5725–5730. https://doi.org/10.1002/anie.201801378
14. Cui Y, Song R, Yu J, Liu M, Wang Z, Wu C, Yang Y, Wang Z, Chen B, Qian G (2015) Dual-emitting MOF supersetdye composite for ratiometric temperature sensing. Adv Mater 27(8):1420–1425. https://doi.org/10.1002/adma.201404700
15. Ma K, Wang H, Li H, Xu B, Tian W (2017) Label-free detection for SNP using AIE probes and carbon nanotubes. Sensors Actuators B Chem 253:92–96. https://doi.org/10.1016/j.snb.2017.06.055
16. Ou X, Zhan S, Sun C, Cheng Y, Wang X, Liu B, Zhai T, Lou X, Xia F (2019) Simultaneous detection of telomerase and miRNA with graphene oxide-based fluorescent aptasensor in living cells and tissue samples. Biosens Bioelectron 124-125:199–204. https://doi.org/10.1016/j.bios.2018.10.009
17. Vedova PD, Ilieva M, Zhurbenko V, Mateiu R, Faralli A, Dufva M, Hansen O (2015) Gold nanoparticle-based sensors activated by external radio frequency fields. Small 11(2):248–256. https://doi.org/10.1002/smll.201401187
18. Bhatnagar D, Kumar V, Kumar A, Kaur I (2016) Graphene quantum dots FRET based sensor for early detection of heart attack in human. Biosens Bioelectron 79:495–499. https://doi.org/10.1016/j.bios.2015.12.083
19. Jesu Raj JG, Quintanilla M, Mahmoud KA, Ng A, Vetrone F, Zourob M (2015) Sensitive detection of ssDNA using an LRET-based upconverting nanohybrid material. ACS Appl Mater Interfaces 7(33):18257–18265. https://doi.org/10.1021/acsami.5b02986
20. Liu S, Bai J, Huo Y, Ning B, Peng Y, Li S, Han D, Kang W, Gao Z (2020) A zirconium-porphyrin MOF-based ratiometric fluorescent biosensor for rapid and ultrasensitive detection of chloramphenicol. Biosens Bioelectron 149:149. https://doi.org/10.1016/j.bios.2019.111801
21. Zhang Q, Wang CF, Lv YK (2018) Luminescent switch sensors for the detection of biomolecules based on metal-organic frameworks. Analyst 143(18):4221–4229. https://doi.org/10.1039/c8an00816g
22. Jeong Y, Kook YM, Lee K, Koh WG (2018) Metal enhanced fluorescence (MEF) for biosensors: general approaches and a review of recent developments. Biosens Bioelectron 111:102–116. https://doi.org/10.1016/j.bios.2018.04.007
23. Akkilic N, Geschwindner S, Hook F (2020) Single-molecule biosensors: recent advances and applications. Biosens Bioelectron 151:111944. https://doi.org/10.1016/j.bios.2019.111944
24. Hermann T (2000) Adaptive recognition by nucleic acid aptamers. Science 287(5454):820–825. https://doi.org/10.1126/science.287.5454.820
25. Liu X, Wang F, Aizen R, Yehezkeli O, Willner I (2013) Graphene oxide/nucleic-acid-stabilized silver nanoclusters: functional hybrid materials for optical aptamer sensing and multiplexed analysis of pathogenic DNAs. J Am Chem Soc 135(32):11832–11839. https://doi.org/10.1021/ja403485r
26. Wang Z, Fu Y, Kang Z, Liu X, Chen N, Wang Q, Tu Y, Wang L, Song S, Ling D, Song H, Kong X, Fan C (2017) Organelle-specific triggered release of immunostimulatory oligonucleotides from intrinsically coordinated DNA-metal-organic frameworks with soluble exoskeleton. J Am Chem Soc 139(44):15784–15791. https://doi.org/10.1021/jacs.7b07895
27. Tian J, Liu Q, Shi J, Hu J, Asiri AM, Sun X, He Y (2015) Rapid, sensitive, and selective fluorescent DNA detection using iron-based metal-organic framework nanorods: synergies of the metal center and organic linker. Biosens Bioelectron 71:1–6. https://doi.org/10.1016/j.bios.2015.04.009
28. Li J, Yuan S, Qin JS, Pang J, Zhang P, Zhang Y, Huang Y, Drake HF, Liu WR, Zhou HC (2020) Stepwise assembly of turn-on fluorescence sensors in multicomponent metal-organic frameworks for in vitro cyanide detection. Angew Chem Int Ed Engl 59(24):9319–9323. https://doi.org/10.1002/anie.202000702
29. Evale BG, Hanagodimath SM (2010) Static and dynamic quenching of biologically active coumarin derivative by aniline in benzene-acetonitrile mixtures. J Lumin 130(8):1330–1337. https://doi.org/10.1016/j.jlumin.2010.03.011
30. Zadran S, Standley S, Wong K, Otiniano E, Amighi A, Baudry M (2012) Fluorescence resonance energy transfer (FRET)-based biosensors: visualizing cellular dynamics and bioenergetics. Appl Microbiol Biotechnol 96(4):895–902. https://doi.org/10.1007/s00253-012-4449-6
31. Wu J, Liu W, Ge J, Zhang H, Wang P (2011) New sensing mechanisms for design of fluorescent chemosensors emerging in recent years. Chem Soc Rev 40(7):3483–3495. https://doi.org/10.1039/c0cs00224k
32. Hu Z, Deibert BJ, Li J (2014) Luminescent metal-organic frameworks for chemical sensing and explosive detection. Chem Soc Rev 43(16):5815–5840. https://doi.org/10.1039/c4cs00010b
33. Ma H, He C, Li X, Ablikim O, Zhang S, Zhang M (2016) A fluorescent probe for TNP detection in aqueous solution based on joint properties of intramolecular charge transfer and aggregation-induced enhanced emission. Sensors Actuators B Chem 230:746–752. https://doi.org/10.1016/j.snb.2016.02.112
34. Zu F, Yan F, Bai Z, Xu J, Wang Y, Huang Y, Zhou X (2017) The quenching of the fluorescence of carbon dots: a review on mechanisms and applications. Microchim Acta 184(7):1899–1914. https://doi.org/10.1007/s00604-017-2318-9
35. Wu Y, Han J, Xue P, Xu R, Kang Y (2015) Nano metal-organic framework (NMOF)-based strategies for multiplexed microRNA detection in solution and living cancer cells. Nanoscale 7(5):1753–1759. https://doi.org/10.1039/c4nr05447d
36. Zhang HT, Zhang JW, Huang G, Du ZY, Jiang HL (2014) An amine-functionalized metal-organic framework as a sensing platform for DNA detection. Chem Commun 50(81):12069–12072. https://doi.org/10.1039/c4cc05571c
37. Xu P, Liao G (2018) A novel fluorescent biosensor for adenosine triphosphate detection based on a metal(-)organic framework

coating polydopamine layer. Materials 11(9). https://doi.org/10.3390/ma11091616

38. Tan H, Tang G, Wang Z, Li Q, Gao J, Wu S (2016) Magnetic porous carbon nanocomposites derived from metal-organic frameworks as a sensing platform for DNA fluorescent detection. Anal Chim Acta 940:136–142. https://doi.org/10.1016/j.aca.2016.08.024
39. He J, Li G, Hu Y (2017) Aptamer-involved fluorescence amplification strategy facilitated by directional enzymatic hydrolysis for bioassays based on a metal-organic framework platform: highly selective and sensitive determination of thrombin and oxytetracycline. Microchim Acta 184(7):2365–2373. https://doi.org/10.1007/s00604-017-2263-7
40. Pan Y, Zhan S, Xia F (2018) Zeolitic imidazolate framework-based biosensor for detection of HIV-1 DNA. Anal Biochem 546:5–9. https://doi.org/10.1016/j.ab.2018.01.017
41. Huang X, He Z, Guo D, Liu Y, Song J, Yung BC, Lin L, Yu G, Zhu JJ, Xiong Y, Chen X (2018) "Three-in-one" nanohybrids as synergistic nanoquenchers to enhance no-wash fluorescence biosensors for ratiometric detection of cancer biomarkers. Theranostics 8(13):3461–3473. https://doi.org/10.7150/thno.25179
42. Xie BP, Qiu GH, Hu PP, Liang Z, Liang YM, Sun B, Bai LP, Jiang ZH, Chen JX (2018) Simultaneous detection of dengue and zika virus RNA sequences with a three-dimensional Cu-based zwitterionic metal-organic framework, comparison of single and synchronous fluorescence analysis. Sensors Actuators B Chem 254:1133–1140. https://doi.org/10.1016/j.snb.2017.06.085
43. Yang W, Zhang G, Weng W, Qiu B, Guo L, Lin Z, Chen G (2014) Signal on fluorescence biosensor for MMP-2 based on FRET between semiconducting polymer dots and a metal organic framework. RSC Adv 4(102):58852–58857. https://doi.org/10.1039/c4ra12478b
44. Yang Q, Zhou L, Wu YX, Zhang K, Cao Y, Zhou Y, Wu D, Hu F, Gan N (2018) A two dimensional metal-organic framework nanosheets-based fluorescence resonance energy transfer aptasensor with circular strand-replacement DNA polymerization target-triggered amplification strategy for homogenous detection of antibiotics. Anal Chim Acta 1020:1–8. https://doi.org/10.1016/j.aca.2018.02.058
45. Hu S, Ouyang W, Guo L, Lin Z, Jiang X, Qiu B, Chen G (2017) Facile synthesis of Fe_3O_4/g-C_3N_4/HKUST-1 composites as a novel biosensor platform for ochratoxin A. Biosens Bioelectron 92:718–723. https://doi.org/10.1016/j.bios.2016.10.006
46. Song C, Wang GY, Wang YL, Kong DM, Wang YJ, Li Y, Ruan WJ (2014) A barium based coordination polymer for the activity assay of deoxyribonuclease I. Chem Commun 50(76):11177–11180. https://doi.org/10.1039/c4cc04272g
47. Yang SP, Zhao W, Hu PP, Wu KY, Jiang ZH, Bai LP, Li MM, Chen JX (2017) Lanthanum-based metal-organic frameworks for specific detection of Sudan virus RNA conservative sequences down to single-base mismatch. Inorg Chem 56(24):14880–14887. https://doi.org/10.1021/acs.inorgchem.7b02107
48. Wang GY, Song C, Kong DM, Ruan WJ, Chang Z, Li Y (2014) Two luminescent metal-organic frameworks for the sensing of nitroaromatic explosives and DNA strands. J Mater Chem A 2(7):2213–2220. https://doi.org/10.1039/c3ta14199c
49. Cordova Wong BJ, Xu DM, Bao SS, Zheng LM, Lei J (2019) Hofmann metal-organic framework monolayer nanosheets as an axial coordination platform for biosensing. ACS Appl Mater Interfaces 11(13):12986–12992. https://doi.org/10.1021/acsami.9b00693
50. Zhao HQ, Qiu GH, Liang Z, Li MM, Sun B, Qin L, Yang SP, Chen WH, Chen JX (2016) A zinc(II)-based two-dimensional MOF for sensitive and selective sensing of HIV-1 ds-DNA sequences. Anal Chim Acta 922:55–63. https://doi.org/10.1016/j.aca.2016.03.054
51. Song WJ (2017) Intracellular DNA and microRNA sensing based on metal-organic framework nanosheets with enzyme-free signal amplification. Talanta 170:74–80. https://doi.org/10.1016/j.talanta.2017.02.040
52. Zhao HQ, Yang SP, Ding NN, Qin L, Qiu GH, Chen JX, Zhang WH, Chen WH, Hor TS (2016) A zwitterionic 1D/2D polymer co-crystal and its polymorphic sub-components: a highly selective sensing platform for HIV ds-DNA sequences. Dalton Trans 45(12):5092–5100. https://doi.org/10.1039/c5dt04410c
53. Zhu X, Zheng H, Wei X, Lin Z, Guo L, Qiu B, Chen G (2013) Metal-organic framework (MOF): a novel sensing platform for biomolecules. Chem Commun 49(13):1276–1278. https://doi.org/10.1039/c2cc36661d
54. Ye T, Liu Y, Luo M, Xiang X, Ji X, Zhou G, He Z (2014) Metal-organic framework-based molecular beacons for multiplexed DNA detection by synchronous fluorescence analysis. Analyst 139(7):1721–1725. https://doi.org/10.1039/c3an02077k
55. Chen L, Zheng H, Zhu X, Lin Z, Guo L, Qiu B, Chen G, Chen ZN (2013) Metal-organic frameworks-based biosensor for sequence-specific recognition of double-stranded DNA. Analyst 138(12):3490–3493. https://doi.org/10.1039/c3an00426k
56. Zhao M, Wang Y, Ma Q, Huang Y, Zhang X, Ping J, Zhang Z, Lu Q, Yu Y, Xu H, Zhao Y, Zhang H (2015) Ultrathin 2D metal-organic framework nanosheets. Adv Mater 27(45):7372–7378. https://doi.org/10.1002/adma.201503648
57. Qiu Q, Chen H, Ying S, Sharif S, You Z, Wang Y, Ying Y (2019) Simultaneous fluorometric determination of the DNAs of Salmonella enterica, Listeria monocytogenes and Vibrio parahemolyticus by using an ultrathin metal-organic framework (type Cu-TCPP). Mikrochim Acta 186(2):93. https://doi.org/10.1007/s00604-019-3226-y
58. Xu C, Liu H, Li D, Su JH, Jiang HL (2018) Direct evidence of charge separation in a metal-organic framework: efficient and selective photocatalytic oxidative coupling of amines via charge and energy transfer. Chem Sci 9(12):3152–3158. https://doi.org/10.1039/c7sc05296k
59. Xu HQ, Hu J, Wang D, Li Z, Zhang Q, Luo Y, Yu SH, Jiang HL (2015) Visible-light photoreduction of CO_2 in a metal-organic framework: boosting electron-hole separation via electron trap states. J Am Chem Soc 137(42):13440–13443. https://doi.org/10.1021/jacs.5b08773
60. Hao YB, Shao ZS, Cheng C, Xie XY, Zhang J, Song WJ, Wang HS (2019) Regulating fluorescent aptamer-sensing behavior of zeolitic imidazolate framework (ZIF-8) platform via lanthanide ion doping. ACS Appl Mater Interfaces 11:31755–31762. https://doi.org/10.1021/acsami.9b12253
61. Fang JM, Leng F, Zhao XJ, Hu XL, Li YF (2014) Metal-organic framework MIL-101 as a low background signal platform for label-free DNA detection. Analyst 139(4):801–806. https://doi.org/10.1039/c3an01975f
62. Qiu GH, Weng ZH, Hu PP, Duan WJ, Xie BP, Sun B, Tang XY, Chen JX (2018) Synchronous detection of ebolavirus conserved RNA sequences and ebolavirus-encoded miRNA-like fragment based on a zwitterionic copper (II) metal-organic framework. Talanta 180:396–402. https://doi.org/10.1016/j.talanta.2017.12.045
63. Qiu GH, Lu WZ, Hu PP, Jiang ZH, Bai LP, Wang TR, Li MM, Chen JX (2017) A metal-organic framework based PCR-free biosensor for the detection of gastric cancer associated microRNAs. J Inorg Biochem 177:138–142. https://doi.org/10.1016/j.jinorgbio.2017.08.036
64. Wei X, Zheng L, Luo F, Lin Z, Guo L, Qiu B, Chen G (2013) Fluorescence biosensor for the H_5N_1 antibody based on a metal-

organic framework platform. J Mater Chem B 1(13):1812–1817. https://doi.org/10.1039/c3tb00501a
65. Wang C, Tang G, Tan H (2018) Pyrophosphate ion-triggered competitive displacement of ssDNA from a metal-organic framework and its application in fluorescent sensing of alkaline phosphatase. J Mater Chem B 6(46):7614–7620. https://doi.org/10.1039/c8tb02175a
66. Ravikumar A, Panneerselvam P (2019) A novel fluorescent sensing platform based on metal-polydopamine frameworks for the dual detection of kanamycin and oxytetracycline. Analyst 144(7):2337–2344. https://doi.org/10.1039/c8an02363h
67. Yang Q, Hong JC, Wu YX, Cao YT, Wu DZ, Hu FT, Gan N (2019) A multicolor fluorescence nanoprobe platform using two-dimensional metal organic framework nanosheets and double stirring bar assisted target replacement for multiple bioanalytical applications. ACS Appl Mater Interfaces 11(44):41506–41515. https://doi.org/10.1021/acsami.9b12475
68. Ravikumar A, Panneerselvam P, Morad N (2018) Metal-polydopamine framework as an effective fluorescent quencher for highly sensitive detection of Hg(II) and Ag(I) ions through exonuclease III activity. ACS Appl Mater Interfaces 10(24): 20550–20558. https://doi.org/10.1021/acsami.8b05041
69. Marieeswaran M, Panneerselvam P (2020) A magnetic nanoscale metal-organic framework (MNMOF) as a viable fluorescence quencher material for ssDNA and for the detection of mercury ions via a novel quenching-quenching mechanism. RSC Adv 10(7):3705–3714. https://doi.org/10.1039/c9ra08274c
70. Li W, Qi X, Zhao CY, Xu XF, Tang AN, Kong DM (2017) A rapid and facile detection for specific small-sized amino acids based on target-triggered destruction of metal organic frameworks. ACS Appl Mater Interfaces 9(1):236–243. https://doi.org/10.1021/acsami.6b13998
71. Chen ML, Chen JH, Ding L, Xu Z, Wen L, Wang LB, Cheng YH (2017) Study of the detection of bisphenol a based on a nano-sized metal-organic framework crystal and an aptamer. Anal Methods 9(6):906–909. https://doi.org/10.1039/c6ay03151j
72. Sun X, Wang Y, Zhang L, Liu S, Zhang M, Wang J, Ning B, Peng Y, He J, Hu Y, Gao Z (2020) CRISPR-cas9 triggered two-step isothermal amplification method for *E. coli* O157:H7 detection based on a metal-organic framework platform. Anal Chem 92(4):3032–3041. https://doi.org/10.1021/acs.analchem.9b04162
73. Zhou W, Hu K, Kwee S, Tang L, Wang Z, Xia J, Li X (2020) Gold nanoparticle aggregation-induced quantitative photothermal biosensing using a thermometer: a simple and universal biosensing platform. Anal Chem 92(3):2739–2747. https://doi.org/10.1021/acs.analchem.9b04996
74. Wang HS, Liu HL, Wang K, Ding Y, Xu JJ, Xia XH, Chen HY (2017) Insight into the unique fluorescence quenching property of metal-organic frameworks upon DNA binding. Anal Chem 89(21):11366–11371. https://doi.org/10.1021/acs.analchem.7b02256
75. Xia Q, Wang H, Huang B, Yuan X, Zhang J, Zhang J, Jiang L, Xiong T, Zeng G (2019) State-of-the-art advances and challenges of iron-based metal organic frameworks from attractive features, synthesis to multifunctional applications. Small 15(2):e1803088. https://doi.org/10.1002/smll.201803088
76. Zhao M, Lu Q, Ma Q, Zhang H (2017) Two-dimensional metal-organic framework nanosheets. Small Methods 1(1–2). https://doi.org/10.1002/smtd.201600030
77. Liu W, Yin R, Xu X, Zhang L, Shi W, Cao X (2019) Structural engineering of low-dimensional metal-organic frameworks: synthesis, properties, and applications. Adv Sci 6(12):1802373. https://doi.org/10.1002/advs.201802373
78. Otsubo K, Haraguchi T, Kitagawa H (2017) Nanoscale crystalline architectures of Hofmann-type metal–organic frameworks. Coord Chem Rev 346:123–138. https://doi.org/10.1016/j.ccr.2017.03.022
79. Murphy MJ, Zenere KA, Ragon F, Southon PD, Kepert CJ, Neville SM (2017) Guest programmable multistep spin crossover in a porous 2-D Hofmann-type material. J Am Chem Soc 139(3): 1330–1335. https://doi.org/10.1021/jacs.6b12465
80. Zhang Y, Qu S, Xu L (2019) Progress in the study of virus detection methods: the possibility of alternative methods to validate virus inactivation. Biotechnol Bioeng 116(8):2095–2102. https://doi.org/10.1002/bit.27003
81. Yang SP, Chen SR, Liu SW, Tang XY, Qin L, Qiu GH, Chen JX, Chen WH (2015) Platforms formed from a three-dimensional Cu-based zwitterionic metal-organic framework and probe ss-DNA: selective fluorescent biosensors for human immunodeficiency virus 1 ds-DNA and Sudan virus RNA sequences. Anal Chem 87(24):12206–12214. https://doi.org/10.1021/acs.analchem.5b03084
82. Qin L, Lin LX, Fang ZP, Yang SP, Qiu GH, Chen JX, Chen WH (2016) A water-stable metal-organic framework of a zwitterionic carboxylate with dysprosium: a sensing platform for ebolavirus RNA sequences. Chem Commun 52(1):132–135. https://doi.org/10.1039/c5cc06697b
83. Tavallaie R, McCarroll J, Le Grand M, Ariotti N, Schuhmann W, Bakker E, Tilley RD, Hibbert DB, Kavallaris M, Gooding JJ (2018) Nucleic acid hybridization on an electrically reconfigurable network of gold-coated magnetic nanoparticles enables microRNA detection in blood. Nat Nanotechnol 13(11):1066–1071. https://doi.org/10.1038/s41565-018-0232-x
84. Gupta A, Bahal R, Gupta M, Glazer PM, Saltzman WM (2016) Nanotechnology for delivery of peptide nucleic acids (PNAs). J Control Release 240:302–311. https://doi.org/10.1016/j.jconrel.2016.01.005
85. Wu L, Qu X (2015) Cancer biomarker detection: recent achievements and challenges. Chem Soc Rev 44(10):2963–2997. https://doi.org/10.1039/c4cs00370e
86. Wu S, Han Y, Wang L, Li J, Sun Z, Zhang M, Liu P, Li G (2019) Sensor array fabricated with nanoscale metal-organic frameworks for the histopathological examination of colon cancer. Anal Chem 91(16):10772–10778. https://doi.org/10.1021/acs.analchem.9b02381
87. Liu X, Zou L, Yang X, Wang Q, Zheng Y, Geng X, Liao G, Nie W, Wang K (2019) Point-of-care assay of alkaline phosphatase enzymatic activity using a thermometer or temperature discoloration sticker as readout. Anal Chem 91(12):7943–7949. https://doi.org/10.1021/acs.analchem.9b01883
88. Zeissig S, Blumberg RS (2014) Life at the beginning: perturbation of the microbiota by antibiotics in early life and its role in health and disease. Nat Immunol 15(4):307–310. https://doi.org/10.1038/ni.2847
89. Gaudin V (2017) Advances in biosensor development for the screening of antibiotic residues in food products of animal origin—a comprehensive review. Biosens Bioelectron 90:363–377. https://doi.org/10.1016/j.bios.2016.12.005
90. De Acha N, Elosua C, Corres JM, Arregui FJ (2019) Fluorescent sensors for the detection of heavy metal ions in aqueous media. Sensors 19(3). https://doi.org/10.3390/s19030599
91. Huang J, Gao X, Jia J, Kim JK, Li Z (2014) Graphene oxide-based amplified fluorescent biosensor for Hg^{2+} detection through hybridization chain reactions. Anal Chem 86(6):3209–3215. https://doi.org/10.1021/ac500192r
92. Feng Y, Shao X, Huang K, Tian J, Mei X, Luo Y, Xu W (2018) Mercury nanoladders: a new method for DNA amplification, signal identification and their application in the detection of Hg(II) ions. Chem Commun 54(58):8036–8039. https://doi.org/10.1039/c8cc03851a

93. Zhao SN, Wu LL, Feng J, Song SY, Zhang HJ (2016) An ideal detector composed of a 3D Gd-based coordination polymer for DNA and Hg^{2+} ion. Inorg Chem Front 3(3):376–380. https://doi.org/10.1039/c5qi00252d
94. Hu PP, Liu N, Wu KY, Zhai LY, Xie BP, Sun B, Duan WJ, Zhang WH, Chen JX (2018) Successive and specific detection of Hg^{2+} and I^- by a DNA@MOF biosensor: experimental and simulation studies. Inorg Chem 57(14):8382–8389. https://doi.org/10.1021/acs.inorgchem.8b01051
95. Chen HL, Li RT, Wu KY, Hu PP, Zhang Z, Huang NH, Zhang WH, Chen JX (2020) Experimental and theoretical validations of a one-pot sequential sensing of Hg^{2+} and biothiols by a 3D Cu-based zwitterionic metal-organic framework. Talanta 210:120596. https://doi.org/10.1016/j.talanta.2019.120596
96. Huang NH, Li RT, Fan C, Wu KY, Zhang Z, Chen JX (2019) Rapid sequential detection of Hg^{2+} and biothiols by a probe DNA-MOF hybrid sensory system. J Inorg Biochem 197:110690. https://doi.org/10.1016/j.jinorgbio.2019.04.004
97. Wang L, Zhi WJ, Lian DS, Wang Y, Han J, Wang Y (2019) HRP@ZIF-8/DNA hybrids: functionality integration of ZIF-8 via biomineralization and surface absorption. ACS Sustain Chem Eng 7(17):14611–14620. https://doi.org/10.1021/acssuschemeng.9b02348
98. Vigderman L, Khanal BP, Zubarev ER (2012) Functional gold nanorods: synthesis, self-assembly, and sensing applications. Adv Mater 24(36):4811–4841, 5014. https://doi.org/10.1002/adma.201201690
99. Liu S, Huo Y, Kang W, Gao Z (2020) Recent advances in surface-enhanced Raman spectroscopy for the detection of tumor markers. Chin Sci Bull 65(15):1448–1462. https://doi.org/10.1360/tb-2019-0640
100. Wang HS, Li J, Li JY, Wang K, Ding Y, Xia XH (2017) Lanthanide-based metal-organic framework nanosheets with unique fluorescence quenching properties for two-color intracellular adenosine imaging in living cells. NPG Asia Mater 9(3):e354–e354. https://doi.org/10.1038/am.2017.7
101. Zhu L, Wong BJC, Li Y, Xin H, Liu B, Lei J (2019) Quencher-delocalized emission strategy of aiegen-based metal-organic framework for profiling of subcellular glutathione. Chemistry 25(18):4665–4669. https://doi.org/10.1002/chem.201900151
102. Liu Y, Hou W, Xia L, Cui C, Wan S, Jiang Y, Yang Y, Wu Q, Qiu L, Tan W (2018) ZrMOF nanoparticles as quenchers to conjugate DNA aptamers for target-induced bioimaging and photodynamic therapy. Chem Sci 9(38):7505–7509. https://doi.org/10.1039/c8sc02210k
103. Park J, Jiang Q, Feng D, Mao L, Zhou HC (2016) Size-controlled synthesis of porphyrinic metal-organic framework and functionalization for targeted photodynamic therapy. J Am Chem Soc 138(10):3518–3525. https://doi.org/10.1021/jacs.6b00007
104. Ulbrich K, Holá K, Šubr V, Bakandritsos A, Tuček J, Zbořil R (2016) Targeted drug delivery with polymers and magnetic nanoparticles: covalent and noncovalent approaches, release control, and clinical studies. Chem Rev 116(9):5338–5431. https://doi.org/10.1021/acs.chemrev.5b00589
105. Lismont M, Dreesen L, Wuttke S (2017) Metal-organic framework nanoparticles in photodynamic therapy: current status and perspectives. Adv Funct Mater 27(14). https://doi.org/10.1002/adfm.201606314
106. Duan W, Zhao Z, An H, Zhang Z, Cheng P, Chen Y, Huang H (2019) State-of-the-art and prospects of biomolecules: incorporation in functional metal-organic frameworks. Top Curr Chem 377(6):34. https://doi.org/10.1007/s41061-019-0258-z
107. Miller SE, Teplensky MH, Moghadam PZ, Fairen-Jimenez D (2016) Metal-organic frameworks as biosensors for luminescence-based detection and imaging. Interface Focus 6(4):20160027. https://doi.org/10.1098/rsfs.2016.0027
108. Zhou J, Tian G, Zeng L, Song X, Bian XW (2018) Nanoscaled metal-organic frameworks for biosensing, imaging, and cancer therapy. Adv Healthc Mater 7(10):e1800022. https://doi.org/10.1002/adhm.201800022